P2X7 Receptor Promotes Mouse Mammary Cancer Cell Invasiveness and Tumour Progression, and Is a Target for Anticancer Treatment

Lucie Brisson, Stéphanie Chadet, Osbaldo Lopez-Charcas, Bilel Jelassi, David Ternant, Julie Chamouton, Stephanie Lerondel, Alain Le Pape, Isabelle Couillin, Aurélie Gombault, et al.

Title page **Research Article**

P2X7 RECEPTOR PROMOTES MAMMARY CANCER CELL INVASIVENESS AND TUMOUR PROGRESSION, AND IS A TARGET FOR ANTICANCER TREATMENTS

Lucie BRISSON[2], Stéphanie CHADET[1], Bilel JELASSI[1], David TERNANT[1], Julie CHAMOUTON[2], Stéphanie LERONDEL[3], Alain LE PAPE[3], Isabelle COUILLIN[4], Aurélie GOMBAULT[4], Fabrice TROVERO[5], Stéphan CHEVALIER[2], Pierre BESSON[1], Lin-Hua JIANG[1,6,7] & Sébastien ROGER[1,8§]

[1] University of Tours, EA4245 Transplantation, Immunology, Inflammation, Tours, France
[2] Inserm UMR1069, Nutrition, Growth and Cancer, University of Tours, Tours, France
[3] CNRS UPS44 TAAM, PHENOMIN, Centre d'Imagerie du Petit animal, Orléans, France
[4] CNRS UMR7355, University of Orléans, Orléans, France
[5] Key-Obs, Orléans, France
[6] School of Biomedical Sciences, Faculty of Biological Sciences, University of Leeds, Leeds, United Kingdom
[7] Sino-UK Joint Laboratory of Brain Function and Injury and Department of Physiology and Neurobiology, Xinxiang Medical University, China
[8] Institut Universitaire de France, Paris, France

Correspondence should be addressed to:
Dr. Sébastien Roger,
EA4245 Transplantation, Immunology, Inflammation,
10 Boulevard Tonnellé, 37032 Tours, France,
Tel: (+33) 2 47 36 61 30, Email: sebastien.roger@univ-tours.fr

Running head: P2X7 is a target for breast cancer treatment

Key words: P2X7 receptor, cancer cell invasiveness, invadopodia, metastases, antagonists

Abstract (max 150 words, count 149)

The P2X7 receptor is an ATP-gated cation channel with a still ambiguous role in cancer progression, proposed to be either pro- or anti-cancerous, depending on the cancer or cell type in the tumour. Here, we show that P2X7 is functional in highly aggressive mammary cancer cells, and demonstrate that it induces a change in cancer cell morphology with fast F-actin reorganization and formation of filopodia, and promotes cancer cell invasiveness through both 2- and 3-dimensional extracellular matrices *in vitro*. Furthermore, P2X7 sustains Cdc42 activity and the acquisition of a mesenchymal phenotype. In an immunocompetent mouse mammary cancer model we demonstrate that the expression of P2X7 in cancer cells, but not in the host mice, promotes tumour growth and metastasis development, which could be reduced by the use of specific pharmacological antagonists. Our results reveal that P2X7 drives mammary tumour progression and is a pertinent target for mammary cancer treatment.

Introduction

The P2X7 receptor belongs to the family of ATP-gated P2X ionotropic receptors which are cation selective channels, permeable to Na^+, Ca^{2+} and K^+ ions [1]. However, since the very beginning of its characterization [2], P2X7 receptor demonstrated several functional and biological specificities differing largely from the other members of the P2X family [3]. From a pharmacological point of view, a specific feature of P2X7 receptor is to be 10~100 times less sensitive to its natural agonist ATP than all other P2X receptors, requiring millimolar concentrations to show sizeable activation while all the others are activated by micromolar concentrations. In addition, P2X7 receptor is about 10~30 times more sensitive to the synthetic BzATP than to ATP [4]. A unique functional property of P2X7 receptor is that it does not demonstrate any negative feedback in its activity. Indeed, while all other members of the P2X family show a more or less rapid decrease of plasma membrane activity following agonist stimulation, a property called desensitisation, the ionic currents produced by P2X7 receptor not only display no reduction, but instead show a facilitation property (also called sensitization). Facilitation was characterized by an increase in current densities and an enhanced sensitivity to the agonist [5-7]. This unique property results in a potentiation of signalling pathways initiated by the receptor.

While all other P2X receptors are mainly expressed in the nervous system, such as in neurons and glial cells, participating to modulation of synaptic transmission, the P2X7 receptor is mostly characterized by its critical participation in immune cells, in immunity and in the inflammatory response [8,9]. In the context of the cancer disease, the P2X7 receptor has attracted escalating attention as well as multiple controversies over the past years. P2X7 was demonstrated to be overexpressed in different types of tumours, such as in brain tumours [10,11], in leukaemia and lymphomas [12] and in carcinomas (such as in breast cancer) [13], with the possible exception of cervical and endometrial cancers in which it was reported to be down-regulated [14,15]. Many studies in favour of the pro-cancerous role of P2X7 activity proposed that its activity led to various properties, such as protecting cells from apoptosis [16], promoting cancer cell trophic activity and

primary tumour growth [17,18] or cell migration or invasion [19-24]. These studies suggest that the use of P2X7 antagonists could be novel and promising anticancer drugs [25]. However, some other studies proposed that P2X7 receptor activation may be anti-cancerous and induces cancer cell death upon ATP stimulation [26-28] or even that P2X7 activity in the host organism is critical to enhance anti-tumour immune response [29-32]. These contrasting roles of P2X7 receptor in cancer promotion probably depend on the type of cancers or tumours, the level of expression or activation, of the receptor, the cell type considered (cancer cells *vs.* immune cells), the level of immune cell infiltration in the tumour, and the phase in the carcinogenic progression. Therefore, from these opposing results it remains unclear whether it would be beneficial or detrimental to antagonize P2X7 receptor for reducing tumour progression, and this should be addressed in specific cancer models.

In breast cancer, P2X7 receptor has been shown to be overexpressed [33] and proposed to promote cancer progression, because of its important contribution to cancer cell invasiveness [21,34,35]. It has been shown that P2X7 receptor was fully functional and promoted cancer cell invasiveness, both *in vitro* and in an *in vivo* zebrafish model, through the release of active cathepsins [21]. This proteolytic activity of cancer cells suggests the involvement of P2X7 receptor in the "mesenchymal mode" of invasion, in which cells generate their path through the extracellular matrix (ECM) by remodelling it. This proteolytic activity is further proposed to be performed by particular cellular structures, enriched in F-actin and protrusive into the ECM, called "invadopodia" [36].

In this study, we assessed the role of P2X7 receptor in the invasive properties in 2- and 3-dimensions models, more specifically in invadopodial activity, and characterized its involvement in the acquisition of a mesenchymal phenotype of mammary cancer cells *in vitro*. We also assessed the consequences of P2X7 expression on primary tumour growth and metastatic spreading *in vivo*. This study also aimed at clarifying the relevance of pharmacological intervention using P2X7 specific antagonists in the treatment of mammary cancers. For this purpose, we developed an orthotopic, syngeneic and immunocompetent mammary cancer model in BALB/cJ mice, and studied the role of

P2X7 receptor, expressed or not in 4T1 mammary cancer cells (using genetically engineered cells) or in the host organisms (wild-type *P2rx7*$^{+/+}$ *versus* knock-down *P2rx7*$^{-/-}$ mice). Our results unequivocally demonstrate that P2X7 receptor is expressed and functional in mammary cancer cells, that its activation promotes the acquisition of a mesenchymal phenotype and enhances invadopodial activity. Furthermore, the P2X7 receptor expressed in mammary cancer cells importantly contributes to primary tumour growth and metastatic development, while its expression in the host organism is not critical, and was significantly reduced by the use of specific pharmacological antagonists.

Results

P2X7 receptor promotes 2- and 3-dimensional mammary cancer cell invasiveness

The expression of P2X7 receptor and its important role in mammary cancer cell invasiveness has initially been documented in the human MDA-MB-435s cell line [21]. However, for the purposes of this study, we aimed at developing a mammary cancer model in immunocompetent mice. Therefore, we investigated the expression and activity of P2X receptors in the 4T1 mammary cancer cell line, originating from the BALB/cJ mouse strain [37]. As shown in Fig. 1a, 4T1 cells expressed mRNA transcripts for P2X2, P2X3, P2X4 and P2X7. A weak band can be visualized for P2X5. The protein expression of these receptors and their functionality at the plasma membrane of cancer cells were assessed using the patch-clamp recording technique. Stimulating the cells with 10 μM ATP, a concentration that would activate all P2X receptors with the exception of P2X7 receptor, did not produce any measurable currents. However, exposure to 5 mM ATP triggered the appearance of an inward, non-desensitizing, facilitating current (Suppl. Fig. 1a) that was inhibited by P2X7 receptor-specific competitive antagonist A438079 [38] (Fig. 1b). These initial results suggest that only P2X7 receptor might be functional at the plasma membrane of 4T1 cells, while other P2X (P2X2 P2X3, P2X4 and P2X5) would be neither expressed at the protein level nor function at the plasma membrane. To further characterize the ATP-induced currents, we performed an ATP dose-response protocol on ionic currents that indicated an EC_{50} of 4.3 ± 0.2 mM (Fig. 1c), consistent with the activity of the mouse P2X7 receptor. The activity of the Ca^{2+}-permeant P2X7 receptor ion channel in 4T1 cells was further studied by monitoring the intracellular Ca^{2+} levels using Fura2 fluorimetry upon ATP (Suppl. Fig. 1b) or BzATP stimulation (Fig. 1d). Both ATP and BzATP induced a biphasic increase in intracellular Ca^{2+} levels in cells incubated in an extracellular saline solution containing 3 mM Ca^{2+}, with a primary transient component followed by a long-lasting one. The long-lasting Ca^{2+} increase was partially reduced in the presence of A438079, coherent with P2X7-mediated Ca^{2+} entry. Similarly to A438079, the non-competitive P2X7 antagonist

AZ10606120 [39] also reduced the long-lasting Ca^{2+} increase induced by BzATP in 4T1 cells, in the presence of extracellular Ca^{2+} (Fig. 1e). The transient, but not the long-lasting, component was also triggered when cells were incubated in the extracellular Ca^{2+}-free solution (Fig. 1d-e, Suppl. Fig. 1b). In this condition, both A438079 and AZ10606120 were ineffective to reduce the intracellular Ca^{2+} increase, thus indicating the activity of ATP- and BzATP-sensitive G-coupled P2Y receptors in 4T1 cells. The P2Y11 receptor, which was reported in cancer cells [40], is known to be sensitive to both ATP and BzATP [41] and is thus a good candidate for this ATP/BzATP-induced intracellular Ca^{2+} increase in the absence of extracellular Ca^{2+}. Indeed, the use of P2Y11 selective antagonist NF340 partially attenuated BzATP-induced intracellular Ca^{2+} increase in Ca^{2+}-free solution (Suppl. Fig. 1c).

To explore the role of the P2X7 receptor in cancer cell biology, we first assessed the effects of increasing ATP concentrations, from 0.03 to 3 mM, on 4T1 cell viability. As shown on Fig. 1f, ATP significantly reduced 4T1 cell viability at all doses tested, and such a detrimental effect was not prevented by A438079. These results largely ruled out the participation of P2X7 receptor in this effect and suggest the involvement of other P2 receptors, or even receptors for adenosine, the major product of ATP hydrolysis, in the reduction of cell viability. This effect on cell viability was not observed when using BzATP as an agonist (Fig. 1g). Therefore, to avoid any non-specific effect related to the activation of another purinergic pathway, BzATP was the only agonist used in all the following experiments to stimulate the P2X7 receptor and assess its participation in cancer cell properties. The participation of P2X7 receptor in 4T1 cell invasiveness was first assessed in a 2-D model using invasion filters covered with a film of Matrigel™, as an extracellular matrix (Fig. 1h-i). In cells transfected with a null-target siRNA (siCTL), BzATP enhanced cancer cell invasiveness by a median factor of 1.95. This effect was not observed when cells were transfected with a siRNA specific for *P2rx7* gene (siP2X7, the efficacy of silencing was assessed by RT-qPCR that indicated a reduction of the P2X7 expression of 68.4 ± 1.6%, n = 6) (Fig. 1h). Furthermore, this increase in invasiveness under BzATP stimulation was prevented in non-transfected 4T1 cells by A438079

(Fig. 1i). We then assessed the effect of stimulating the P2X7 receptor on 3D cancer cell invasiveness. Spheroids composed of 4T1 cells were grown in a 3D matrix of Matrigel™ for 72 h (Fig. 1j). 4T1 cells are very cohesive cells, tending to invade under a collective mode, rather than under an individual mode. Therefore, we measured the circularity index of spheroids, which is inversely correlated to the invasiveness, in the different treatment conditions. As shown in Fig. 1j, BzATP reduced the spheroid circularity, indicating a gain in invasiveness, and the BzATP-induced reduction of circularity was prevented in the presence of A438079. By comparison, similar spheroids experiments were performed using MDA-MB-435s human cancer cells, which tend to invade matrices under an individual cell mode (Suppl. Fig 2a). BzATP increased the maximal distance of matrix invasion, which was also prevented by treating the spheroids with A438079 (Suppl. Fig. 2b). These results indicate that P2X7 receptor activity promotes cancer cell invasiveness, regardless of the mode of invasion (collective *vs.* single cell invasion), in both 2D and 3D models.

P2X7 receptor participates to the acquisition of a mesenchymal cancer cell phenotype

Invadopodia are key structures of cancer cell invasiveness, involved in extracellular matrix (ECM) remodelling [42]. Therefore, we analysed the ECM digestive activity of cancer cells grown on a planar matrix of Matrigel™ containing DQ-BSA as a fluorogenic substrate for proteases. Immunofluorescence imaging identified that P2X7 proteins were strongly co-localized with the matrix proteolytic activity (Fig. 2a) in both mouse 4T1 (Pearson's r = 0.64) and human MDA-MB-435s (Pearson's r = 0.62) cancer cells. Since invadopodia are cancer cell structures that are protrusive into the extracellular matrix, it is possible to isolate invadopodia-enriched fractions, from cytosolic or membrane fractions, coming from cancer cells grown on a thick matrix composed of gelatin [43]. Figure 2b shows that the invadopodia fraction from 4T1 cells, characterised by the presence of the invadopodia markers, cortactin, focal adhesion kinase (FAK), cathepsin B (Cath B), also contained P2X7 proteins. Similar results were obtained with human MDA-MB-435s cells (Suppl. Fig. 3a). Invadopodial activity can be characterised by focalized areas of ECM degradation

co-localised with F-actin condensations. To assess a possible regulation of the invadopodial activity by the P2X7 receptor, 4T1 cells were grown on a planar matrix of Matrigel containing DQ-BSA, and F-actin was labelled (Fig. 2c). Areas corresponding to the co-localization of F-actin condensation areas and focal spots of DQ-BSA proteolysis were identified and quantified per cell. Stimulating the cells with BzATP increased the surface of degradation spots, and this was prevented by A438079 (Fig. 2d), whereas the number of invadopodial structures (degradation spots) per cell remained unchanged (Fig. 2e). Similar results were obtained with human MDA-MB-435s cells (Suppl. Fig. 3b-d). These results strongly suggest that P2X7 receptor activity enhances the proteolytic activity of individual invadopodia.

The ECM digestive activity and the presence of invadopodia are specific characteristics of cancer cells showing a "mesenchymal phenotype" [44]. In this phenotype, engaged cells display an elongated fibroblast-like morphology, with a rear-to-front cell polarity, the presence of lamellopodia at the leading edge and multiple filopodial structures all around the cells. Filopodia are F-actin enriched thin structures allowing attachment to the matrix. As shown in Fig 3a, stimulation of 4T1 cells with BzATP induced a rapid change in cell morphology with a remodelling of F-actin cytoskeleton. Cancer cells appeared to be more elongated and the lamellopodia readily visualized. Time-lapse microscopy imaging (see Suppl. Movies 1-4) also showed that BzATP increased the number of filopodial structures per cell, which was prevented by A438079 (Fig. 3b). A438079 alone did not modify the number of filopodia. In contrast, the velocity to form and extend filopodia was not affected (Fig. 3c). The control of cytoskeleton remodelling and the acquisition of invasive phenotypes are orchestrated in cancer cells by members of the Rho-GTPase family [45,46]. Particularly, Cdc42 has been identified to contribute importantly to cancer cell invasion, to the acquisition of a mesenchymal phenotype, and to the formation of invadopodia [47]. Interestingly, BzATP specifically increased the level of the active, GTP-bound form of Cdc42, with no effect on RhoA and Rac1, and this was abrogated by A438079 (Fig. 3d). To further study the participation of P2X7 receptor in the epithelial-to-mesenchymal transition (EMT), we assessed the effect of

stimulating 4T1 cancer cells with BzATP on the expression of genes associated with the mesenchymal (*SNAI1, ZEB1, TWIST*) or the epithelial (*ZO1, CDH1*) phenotypes. This stimulation induced no change in the expression of the mesenchymal transcription factor, but repressed the expression of gene *ZO1* encoding for the epithelial tight junction protein Zonula occludens-1. Stimulating cells with BzATP had no effect on the expression of *CDH1*, encoding for E-cadherin (Fig. 3e). Taken together, these results identify the P2X7 receptor as a strong promoter of invadopodial activity that participates to maintain a mesenchymal aggressive phenotype in cancer cells without being critical to the induction of EMT.

P2X7 receptor enhances mammary tumour growth and metastasis development and is a target for anticancer treatment

In order to assess the role of P2X7 receptor in mammary tumour growth and metastatic progression, we genetically modified 4T1 mouse mammary cancer cells for its expression. These cells, which endogenously express the P2X7 receptor, were modified using the CRISPR/Cas9 gene-editing technique in order to knock down the expression of the *P2rx7* gene. This led to the generation of three cell lines, two of which were named Crispr#1 and Crispr#2 with a *P2rx7* knocked-down efficacy superior to 95%, and one control cell line named CTL expressing the *P2rx7* gene at a level similar to that of the parental 4T1 cells (Fig. 4a). As a result, the Crispr#1 and Crispr#2 cell lines displayed a reduced invasiveness capacity compared to the CTL cell line and, furthermore, no potentiation by BzATP (Fig. 4b). Both Crispr#1 and Crispr#2 cell lines demonstrated a slight increase in proliferation (by a median factor of 1.32 and 1.33, respectively Fig. 4c) and in cell adhesion (by a median factor of 1.19 and 1.15, respectively; Fig. 4d) relative to CTL cells, under basal conditions, *i.e.* without external stimulation of P2X7 receptor with an agonist. These three cell lines demonstrated a luciferase activity that was comparable to that of parental 4T1 cell line (Suppl. Fig. 4a), allowing their use for *in vivo* experiments.

We first aimed at deciphering the role of P2X7 receptor expressed by the cells of an organism hosting a mammary tumour, most importantly those of the immune system, on primary tumour growth and metastasis development. To do so, we implanted CTL cells (null-target CRISPR/Cas9-processed 4T1-Luc clone endogenously expressing the *P2rx7* gene) in the fifth mammary fat-pad of either wild-type *(P2rx7$^{+/+}$)* or in knock-out *(P2rx7$^{-/-}$)* BALB/cJ mice (Fig. 4e). Whatever was the density of cancer cells implanted ($1x10^6$ or $1x10^4$ cells), there was no difference in the mammary tumour growth (Fig. 4f and Fig. 4h, respectively), or in the metastatic development (Fig. 4g and Fig. 4i, respectively), between the *P2rx7*$^{+/+}$ and *P2rx7*$^{-/-}$ mice. These results indicate that in this model, the expression of P2X7 receptor in host cells does not interfere with mammary tumour progression. Therefore, we decided to assess the role of the P2X7 receptor being expressed by cancer cells (Fig. 4j). Loss of the *P2rx7* expression in 4T1 cancer cells strongly reduced mammary tumour growth (Fig. 4k) and also, most probably as a consequence of primary tumour reduction, markedly inhibited the development of metastatic foci (Fig. 4l). The knock-down of *P2rx7* expression in Crispr#1 and Crispr#2 cells remained stable for all the duration of the *in vivo* experiment (Suppl. Fig. 4b) as well as in primary tumours generated by these cells (Suppl. Fig. 4c). Because the presence of P2X7 receptor in cancer cells seemed to promote mammary tumour progression (Fig. 4c), and because the expression of P2X7 in host cells did not reduced it (Fig. 4f-i), we wondered whether the treatment of mice bearing established mammary tumours with P2X7 antagonists would be effective to slow down the tumour growth. Therefore, we injected intraperitoneally wild-type mice, along with either the competitive antagonist A438079, or the non-competitive antagonist AZ10606120, or the vehicle as a control, when primary tumours reached a minimal size of 80 mm^3 (Fig. 5a). Primary tumour growth in the three experimental groups was measured and results indicated a tendency for reduction of tumour growth in presence of P2X7 antagonists (Fig. 5b). This was further studied using a Gompertz mathematical model applied to tumour growth (Fig. 5 c-e). Estimated mean (inter-individual standard deviation) of model parameters were kgrowth = 0.64 day-1 (39%), Vmax = 1,620 mm^3 (64%), EFF = 0.52 (82%) and γ

= 0.17 (–). This analysis shows that in the vehicle group, the tumour volume doubled in a mean time of 0.64 day, and that the mean maximum tumour volume was 1,620 mm^3 (Fig. 5c). Treatments with A438079 (Fig. 5d) and AZ10606120 (Fig. 5e) were both effective, inducing a massive reduction in tumour growth over time by a factor of 2 ($p<10^{-10}$). There was no difference in efficacy between these two treatments ($p = 0.08$), even if a trend toward a better efficacy was detected for AZ10606120. In addition, Vmax was significantly higher for AZ10606120 treatment ($p = 0.0065$), which may not be due to treatment condition, but rather to between-subject variability. In this experiment, we identified no statistically significant difference in the metastatic colonisation (Fig. 5f), but noticed a trend for an increased survival rate for A438079-treated mice that was statistically significant for AZ10606120-treated mice (Fig. 5g). Taken together, these results consistently demonstrate that the expression of P2X7 receptor in mammary cancer cells, but not in host cells, enhances mammary tumour growth and metastasis development and is a target for anticancer treatment.

Discussion

The acquisition of invasive capacities by cancer cells represents a critical mechanism in the progression of the cancer disease, since they importantly participate to the metastatic cascade, and therefore impacts patients' survival [48]. Currently, there is no specific treatment for preventing cancer cell spreading from the primary tumour and no specific treatment for preventing metastases appearance. At the cellular level, several modes of cancer cell migration and invasiveness have been described, both in *in vitro* and *in vivo* models, among which the "amoeboid" and the "mesenchymal" modes, that could be defined as being based on a collective and an individual cell behaviour [49]. Even though these modes of invasion could be more characteristic of some cancer types or subtypes, cancer cells do not stay engaged in one specific mode. Those cells which can be considered the most aggressive ones have the ability to switch from one to other mode, depending on biological, physical and chemical conditions of the microenvironments [50-52]. Whatever the mode of invasion, being individual or collective, the capacity of degrading extracellular matrices allows faster dissemination of cancer cells, and critically depends on the contribution of proteases, such as matrix metalloproteinases (MMP) and cathepsins. This capacity to invade extracellular matrices with a proteolytic degradation was initially described as being a feature of mesenchymal cancer cells. Mesenchymal cancer cells display an elongated fibroblast-like morphology, with a rear-to-front lamellopodial cell polarity, and harbour multiple cell-matrix adhesions, such as filopodial structures. The degradation of the ECM is recognized to be performed by invadosomal structures, which are F-actin-rich organelles, protrusive into the ECM and responsible for its proteolysis through recruiting both membrane-associated and extracellularly-released soluble proteases [36,44].

Extracellular ATP, and derived nucleotides, is known to importantly contribute to the differentiation and activation of multiple cell types, not only under physiological but also in pathological conditions. When released in the extracellular compartment, they activate plasma membrane purinoreceptors and downstream signalling pathways. Over the past few years, the purinergic signalling has attracted considerable attention in the field of oncology [13,53]. Indeed,

concentrations of ATP and other nucleotides have been demonstrated to be highly increased in the tumour microenvironment, owing to the active release of ATP from cancer cells and to cell necrosis in the hypoxic halo of solid tumours [54,55], and the expression or activity of several purinoreceptors is dysregulated in cancer cells. In such conditions, receptors expressed at the plasma membrane can be activated and in turn can activate the associated signalling pathways, and this occurs in the different cell types in the tumour, such as cancer cells of course and also immune cells, fibroblasts and endothelial cells. Obviously, the consequences on tumour and disease progression could be drastically opposite, depending on the cell type considered, and it is indispensable to have a clear vision on the whole disease. The P2X7 receptor is a very intriguing receptor, which has been demonstrated to be upregulated in multiple cancer types [13], but its clear involvement in carcinogenesis or cancer progression is still debated. Because the over-stimulation of P2X7, either in dose or in duration, is known to induce cell death [56], several authors postulated that it might be non-functional in proliferating cancer cells [33,57,58]. It was even proposed that stimulating its activity in cancer cells would induce their death and could represent therapies for treating cancers [59]. However, multiple studies demonstrated that the P2X7 receptor is expressed and functional in cancer cells and that its basal activity or its external stimulation with biologically-compatible doses of ATP support cancer cell growth, migration, invasion [21,22,60], tumour growth [18,23]. In these models, pharmacological antagonism of the P2X7 receptor appeared to be effective in reducing cancer progression, suggesting that pharmacological interventions targeting P2X7 receptor could represent novel anticancer opportunities. On the other hand, the important role of P2X7 receptor in the immune response is well established [9]. Therefore, its expression and activity in cells from the host organism of a tumour might interfere with tumour progression. Importantly, its role in tumour-associated dendritic cells for the presentation of tumour antigen to $CD4^+$ lymphocytes, and its role in anti-tumour immune response were demonstrated [29,61]. Therefore, it was questioned whether P2X7 receptor had a real role in cancer progression, as well as whether using P2X7 antagonists was pertinent and useful for anticancer treatment. In a very nice study, Adinolfi and collaborators

339 demonstrated that, when expressed in mouse melanoma or colon cancer cells subcutaneously
340 inoculated to P2X7-deficient mice, P2X7 receptor strongly promoted tumour growth and metastatic
341 dissemination. However, both primary tumour growth and metastases were reduced in P2X7-
342 expressing wild-type mice because of a P2X7-dependent anti-tumour immune response [62]. Another
343 study, performed in the context of colon cancer, also points out an important role for P2X7 receptor
344 in anti-tumour immune response. In this study, Hofman and collaborators show that
345 pharmacological antagonism or genetic silencing of the P2X7 receptor altered immune cell
346 infiltration and increased tumour incidence in a mouse model of colitis [63]. Therefore, from these
347 studies it appeared that the use of P2X7 antagonists for anti-cancer treatment might be very
348 deleterious and could lead to opposite tumour-promoting effects. Melanoma and colon cancer
349 development and progression are known to be highly dependent on the immune and inflammatory
350 system [64,65]. For other cancers, the question is still open, and the relative participation of P2X7
351 receptor, when expressed by cancer cells or host cells, might be different and should be specifically
352 assessed.

353 In this study, we demonstrated that the P2X7 receptor is functional in 4T1 mouse mammary
354 cancer cells and that its activation with natural (ATP) or synthetic (BzATP) agonists induces typical
355 facilitating inward currents and increases in intracellular Ca^{2+} concentration. Its stimulation did not
356 seem to induce cell death, even though the genetic silencing of the *P2rx7* gene led to a slight
357 increase in the proliferation rate, but instead importantly enhanced 2D and 3D cell invasiveness.
358 These effects were similarly prevented both by the use pharmacological antagonists and by genetic
359 invalidation, indicating that not only the protein P2X7 but its activity promotes invasiveness. These
360 results are in agreement with previous reports performed with human cancer cells [20-22,24,35,66]. While
361 mechanistic determinants for this pro-invasive role were not clearly recognized, we identified for
362 the first time in this study the expression of P2X7 in invadopodial structures involved in ECM
363 degradation. Most specifically, the expression of P2X7 receptor enhanced the ECM-degradative
364 activity of invadopodia, most probably through the release of proteolytic enzymes [21], rather than the

number of these structures *per se*. Activating P2X7 receptor also importantly modified cancer cell morphology and triggered the acquisition of a more aggressive phenotype, characterized by activation of Cdc42 Rho-GTPase, remodelling of F-actin, elongation of cells, and formation of filopodia. Taken together, these results strongly suggest the involvement of P2X7 receptor in promoting the acquisition of a mesenchymal invasive phenotype in mammary cancer cells. Activation of the P2X7 receptor reduced the expression of *ZO-1*, importantly involved in tight junctions and in maintaining the epithelial polarity. However, in our model, activation of the P2X7 receptor did not appear to be a key inducer of EMT. Indeed, there was no significant change in the expression of EMT-promoting transcription factors, Zeb1, Snail1 or Twist, and the expression of the gene encoding for E-cadherin was not modified. These findings seem to be contrasting to recently published studies. In prostate cancer cells, P2X7 receptor promoted invasiveness and metastatic properties and silencing its expression attenuated ATP- or BzATP-driven changes in the expression of EMT-related genes, Snail, E-cadherin and Claudin-1 [24]. Also, in osteosarcoma cells, stimulation of P2X7 receptor reduced the expression of E-cadherin, and induced those of Snail, vimentin and fibronectin. These effects were prevented by pharmacologically antagonizing the receptor or knocking down its expression [66]. However, these differences might depend on the cell types studied and on their level of transition. Indeed, it was demonstrated that murine 4T1 mammary cancer cells, which are highly invasive and metastatic, do not strictly demonstrate genotypic and phenotypic properties of EMT [67]. It was postulated that other processes may govern metastatic capability in these cells. Furthermore, it is know that EMT is not an all-or-nothing phenomenon, and some cancer cells display intermediate or partial transition states that have been identified to be highly aggressive [68].

Here, we investigated the role of P2X7 receptor, whether it was expressed by cancer cells or by host cells, in mammary cancer progression. By using *P2rx7*$^{+/+}$ and *P2rx7*$^{-/-}$ mice, we demonstrated that, in the syngeneic and orthotopic model of mammary cancer, there is no participation of the P2X7 receptor in the host organism in either anti- or pro-tumour activities.

Because the level of the anti-tumour response of the host organism might depend on the size of the primary tumour, we inoculated two different numbers of mammary cancer cells (low density of $1x10^4$ or high density of $1x10^6$ cells per inoculation site) but no difference was observed. This is in apparent contradiction to previously published studies [62,63], but may be due to the specific mammary gland microenvironment [69], as compared to the subcutaneous or colic environments, or to specific anti-immune responses induced by 4T1 cells. This should be clarified in independent studies. However, in stark contrast, the expression and activity of P2X7 receptor in mammary cancer cells had a predominant effect in mammary tumour growth and metastasis development. Loss of the *P2rx7* expression in two cell lines derived from 4T1 cells led to a significant delay in primary tumour growth, while the cells demonstrated a slight increase in the proliferation rate compared to the $P2rx7^{+}/^{+}$ cells. Using two different *P2rx7*-knocked-out clones rules out possible off-targets of the CRISPR/Cas9 technique used and demonstrates the critical involvement of cancer cell invasiveness in primary tumour growth. We demonstrated a clear reduction of metastatic colonization of organs when cancer cells did not express the *P2rx7* gene. However, it is not clear whether this effect is specific or due to the important delay in primary tumour growth. Furthermore, we demonstrated that the use of two P2X7 antagonists, with different modes of action, one being competitive (A438079) while the other is non-competitive (AZ10606120), had similar effects in reducing the tumour growth in wild-type ($P2rx7^{+}/^{+}$) mice.

In conclusion, we have identified the P2X7 receptor in mammary cancer cells as a key molecular determinant of cancer cell invasiveness and mammary tumour growth, and as a possible target for pharmacological interventions.

Methods

Agonists, antagonists, salts and chemicals - Adenosine 5'-triphosphate (ATP) disodium salt and 2'-(3')-O-(4-benzoylbenzoyl)adenosine 5'-triphosphate (BzATP) triethylammonium salt were purchased from Sigma-Aldrich (France) and prepared in PBS without Ca^{2+}. P2X7 selective antagonists, A438079 and AZ10606120, and P2Y11 selective antagonist NF340, were purchased from Tocris Bio-Techne (France) and prepared in saline solution. All salts and pH buffers for electrophysiological solutions were purchased from Sigma-Aldrich (France). Fluorescent probes (Phalloidin DyLight® 488, DQ™-BSA and Fura2-AM) were all purchased from Invitrogen (France).

Cells and cell culture - Human breast cancer cell line MDA-MB-435-luc were constructed as previously described [70]. Murine mammary cancer cell line 4T1 from the Balb/c strain was purchased from LGC Standards (France), and a stable 4T1-luc cell line expressing the luciferase gene (thereafter called "4T1 cells") was obtained by transduction with lentiviral vectors containing the luciferase gene and blasticidin resistance gene for selection (GIGA Viral Vectors, Belgium). Stable 4T1 cell lines knocked-out for the expression of the *P2rx7* gene were obtained using the CRISPR/Cas9 technique by transfection with the *P2rx7* Double Nickase Plasmid (Santa Cruz, France). Clonal selection was performed using 2 µg/ml puromycin. Two clones have been kept for this study, called "Crispr#1" and "Crispr#2". A null-target Double Nickase Plasmid was also used to transfect 4T1 cells and this led to the selection of a control cell line, thereafter called "CTL" cell line. Efficiency of the CRISPR-mediated knock-down was assessed by RT-qPCR and invasion assays, and stability of clones was followed for a minimal duration of 6 weeks. Selected clones displayed similar levels of luciferase activity.

MDA-MB-435-luc cells were grown in Dulbecco's modified Eagle's medium (DMEM) supplemented with 5% foetal calf serum (FCS). All 4T1-derived cells were cultured in RPMI medium supplemented with 10% FCS. Cells were grown at 37°C in a humidified 5% CO_2

441 incubator. Mycoplasma contamination tests were performed routinely (Lonza, MycoAlert™
442 Mycoplasma Detection Kit).

443 ***Small interfering RNA transfection*** – 4T1 mammary cancer cells were transfected with
444 siRNA directed against mouse *P2rx7* mRNA (siP2X7) or scramble siRNA-A as a control (siCTL),
445 both of which were purchased from Tebu-Bio (France). Cells were transfected with 20 nM siRNA
446 by using Lipofectamine RNAi max (Invitrogen, France). Experiments were performed 24 h after
447 transfection and efficacy of silencing was assessed by qPCR.

448 ***RNA extraction, reverse transcription and polymerase chain reaction –*** For conventional
449 PCR experiments, total RNA was extracted using NucleoSpin® RNA II kit (Macherey Nagel
450 EURL, Germany) and reverse transcribed with PrimeScript™ RT Reagent (Ozyme, France). PCR
451 was performed with GoTaq® Flexi DNA Polymerase (Promega, France) according to
452 manufacturer's recommendations. PCR products were loaded on 2% agarose gels and visualised
453 after UV excitation.

454 For real-time qPCR experiments, total RNA was extracted using TRIzol™ Reagent (Invitrogen,
455 France), and reverse-transcribed with the PrimeScript™ RT Reagent Kit (Ozyme, France).
456 Quantitative PCR were performed using SYBR qPCR Premix Ex Taq (Ozyme, France) and CFX
457 CONNECT (Bio-rad, France). Control gene was *mGusb* and primers used were those as described
458 [71]. qPCR primer sequences for assessing m*P2rx7* expression were those previously described [72]. All
459 primers sequences are described in Table I.

460 ***Cell electrophysiology –*** Electrophysiological recordings of ATP-mediated currents were
461 performed in the whole cell configuration of the patch clamp technique as already reported [6]. Patch
462 pipettes were pulled from borosilicate glass (World Precision Instruments, France) to a resistance of
463 4-6 MΩ. Currents were recorded under voltage-clamp mode using an Axopatch 200B amplifier
464 (Axon Instrument, USA) and analogical signals were filtered at 10 kHz and digitized using a 1322A
465 Digidata converter. Cell capacitance and series resistance were electronically compensated.
466 Membrane potential was held at -60 mV. Experiments were performed at room temperature (20-

25°C) in a standard external physiological saline solution (PSS in mM: 147 NaCl, 10 N-2-hydroxyethylpiperazine-N'-2ethansulphonic acid (HEPES), 13 D-glucose, 2 KCl, 2 $CaCl_2$ and 1 $MgCl_2$) and pipettes were filled with the intracellular saline solution (in mM: 147 NaCl, 10 HEPES and 10 ethylene glycol-bis-(2-aminoethyl ether)-N, N, N', N'-tetraacetic acid (EGTA) with osmolarity and pH values of 295-315 mOsm and 7.3, respectively). ATP was externally applied using a RSC160 fast-flow delivery system (BioLogic Science Instruments, France) for 10 s, at the concentrations indicated in the figure legend. P2X7 antagonist A438079 was perfused into the bath for 2 min before recording its effect in the presence of 5 mM ATP. Concentration-response curves to ATP were realized by first obtaining a maximum response to 10 mM and then by applying decreasing concentrations of agonist and the results were plotted using Origin Pro 2015 software (Microcal Software Inc., USA). EC_{50} was defined using the Hill equation provided by the software.

Intracellular calcium measurement **–** ATP- and BzATP-induced intracellular calcium increases were measured using the ratiometric fluorescent probe Fura2-AM and the Flexstation3 apparatus (Molecular Devices) as already described [40]. Cells were incubated with Fura2-AM (1 μM) for 45 min in OptiMEM medium at 37°C prior to conduct recordings. Cells were washed and then pre-incubated in the extracellular saline solution (147 mM NaCl, 2 mM KCl, 1 mM $MgCl_2$, 10 mM HEPES and 13 mM D-glucose, pH 7.4) with and without 3 mM $CaCl_2$. F340/F380 defined the ratio of the fluorescence intensity excited alternatively at 340 nm and 380 nm and emitted at 510 nm and was used to determine the free intracellular Ca^{2+} concentration. It was measured after the injection of either 3 mM ATP or 0.3 mM BzATP. Agonists were added after the baseline was established. Antagonists, A438079 (10 μM) or AZ10606120 (300 nM) were added 5 min before addition of agonist.

Cell viability **–** The effects of ATP and BzATP treatments for 24 h on 4T1 cells, at doses indicated in the figure legends were evaluated by the tetrazolium salt assay (MTT) as already described [21]. Briefly, cells were treated with increasing doses of ATP and BzATP for 24 h and cell viability was measured after incubation with MTT for 40 minutes at 37°C.

493 ***Cell adhesion*** - To assess 4T1 cancer cell adhesion, $2x10^4$ cells were seeded in their normal
494 culture medium in wells from a 96-well plate and placed in the incubator for 30 min at 37°C, 5%
495 CO_2. After one wash in PBS, the number of adherent cells was evaluated in wells using the MTT
496 assay.
497 ***2- and 3-Dimensions in vitro invasion assays*** – 2-D cancer cell invasiveness was measured
498 as previously described [21] using 8-µm pore-size polyethylene terephtalate membrane inserts covered
499 with Matrigel™ matrix (Becton Dickinson, France). Cells at the lower surface of the insert were
500 stained with DAPI and nuclei were counted after collecting pictures with a Nikon TI-S microscope
501 (France). Results were normalized to the control condition, in the absence of agonist or antagonist.
502 For 3D invasiveness assays, cancer cell spheroids were used. To do so, 500 4T1 cells or 2,000
503 MDA-MB-435luc cells were seeded in wells of ultra-low attachment 96-well plates (Corning,
504 France). After allowing spheroid formation at 37°C and 5% CO_2 in the incubator for 24 h for
505 4T1luc and 48 h for MDA-MB-435luc, 4 mg/ml Matrigel™ was added to the wells, in the absence
506 or presence of 0.3 mM BzATP, and 10 µM A438079. 3D-Matrigel invasion by spheroids was
507 followed every hour using a Nikon TI-S microscope (France). Invasion distance and spheroid
508 circularity were measured and calculated using ImageJ.
509 ***Invadopodia activity assay*** - Invadopodia activity was assessed by culturing cells for 24 h
510 on the top of a layer of Matrigel™ (4 mg/mL) matrix containing 50 µg/mL of DQ-BSA in
511 LabTeck™ chambers, as previously reported [43]. Briefly, cells were fixed in 4% paraformaldehyde
512 for 15 min then permeabilized using 0.02% saponin for 20 minutes and incubated with 3% bovine
513 serum albumin (BSA) for 30 min. F-actin was stained with 1.5 units/mL Phalloidin DyLight 488
514 (Invitrogen, France). Slides were mounted using ProLong® Gold Antifade Mountant with DAPI
515 (Invitrogen, France). Epifluorescence microscopy was performed with a Nikon TI-S (France). Co-
516 localized pixels for DQ-BSA and Phalloidin-488 were obtained using NIS-Element (Nikon, France)
517 and fluorescence intensity, as well as the number of invadopodia were quantified with ImageJ.

Invadopodia fractionation – Invadopodia, which were embedded in the gelatin matrix, were separated from cellular bodies using the previously described protocol [43]. Briefly, cells were grown on the top of a 2%-gelatin matrix. Cellular bodies were removed using osmotic shock and further fractionated to isolate a "cytosolic" and an "all membranes" fractions. Proteins from invadopodia were solubilised in a lysis buffer containing 0.1% NP-40 and 1 mM DTT and separated from gelatin by centrifugation at 17,000 x g for 30 min. Proteins in each fraction were separated according to standard SDS-PAGE protocols on 8% and 12% polyacrylamide gels and then transferred on PVDF membrane. Primary antibodies used were: mouse anti-HSC70 (sc-7298 Santa Cruz, Germany), rabbit anti-caveolin 1 (sc-894 Santa Cruz, Germany), rabbit anti-β-adaptin (610382 BD Biosciences, France), cathepsin B (20-CR71 Fitzgerald, USA), cortactin (05-180 Millipore, France), FAK (036SC-558 Santa Cruz, France), P2X7 (APR-008 Alomone, Israel). Secondary HRP-conjugated antibodies were: goat anti-mouse (Santa Cruz, France), goat anti-rabbit (Jackson Immunoresearch Interchim, France), rabbit anti-β-actin-HRP (Santa Cruz, France). Densitometric analyses were performed using ImageJ. Full uncropped blots are shown in Supplementary Figures 5 and 6.

Epifluorescence experiments – Cells were grown for 24 h in LabTeck™ chambers on a layer of Matrigel matrix (4 mg/mL) containing 50 µg/mL of DQ-BSA. Cells were fixed in 4% paraformaldehyde for 15 min and then incubated with 3% BSA for 30 min. P2X7 was immunodetected using a primary antibody (APR-008, Alomone, Israel) and secondary anti-rabbit IgG AlexaFluor488 (Invitrogen, France). For actin cytoskeleton analysis, cells were grown on glass coverslips until 40 % confluency and then serum was reduced to 1% for 24 h and 0% for 24 h. Cells were treated with BzATP for 2, 4, 6, 12, 30 min and 24 h. Cells were fixed in 4% paraformaldehyde for 15 min and then permeabilized with 0.1% triton-X-100 for 5 min, incubated with 3% BSA for 30 min and stained with 1.5 units/mL Phalloidin DyLight® 488 (Invitrogen, France) for 1 h. Slides were mounted using ProLong® Gold Antifade Mountant with DAPI (Invitrogen, France). For the analysis of filopodia, cells were transfected with Ibidi® LifeAct plasmid (Generous gift from Prof.

Laurent Counillon, CNRS UMR7370, University of Nice-Sophia Antipolis) using TransIT®-2020 (Mirus Euromedex, France). Epifluorescence and Time-lapse microscopy was performed with a Nikon TI-S (France) (See supplementary materials SMovie 1-4). Numbers of filopodia formed per hour and filopodia velocity were quantified using the Adapt plugin for ImageJ [73].

RhoGTPases pull-down assays – T*he activity of* RhoA / Rac1 / Cdc42 small GTPases was assessed using pull-down assays according to the manufacturer's protocols (Cat BK030 RhoA/ Rac1/Cdc42 Activation Assay Combo Biochem Kit, Cytoskeleton, Tebu-Bio, France) as previously described [52]. Briefly, cells were grown until 40% confluency in 75-cm² flasks in normal growing medium, and serum was reduced to 1% for 24 h and 0% for 24 h. After treatment with 0.3 mM BzATP with or without 10 µM A438079 for 30 min in culture medium without serum, cells were lysed and samples were snap-frozen in liquid nitrogen. For each condition, 500 µg total lysates were used for pull-down assay according to the manufacturer's instructions and then used for western blotting (Full uncropped blots are shown in Supplementary Figure 7).

In vivo mammary cancer model and experiments – All experiments have been approved by the Comité d'éthique du Centre-Val de Loire (Comité d'éthique en expérimentation animale Campus CNRS d'Orléans n°3) and have been performed in accordance with the European Ethics rules (Ref 005377.01 Apafis #12960). All animals were bred and housed in isolated ventilated cages at the CNRS UPS44 – TAAM- CIPA (CNRS Campus, Orléans, France), in controlled conditions with a 12-hr light/dark cycle at 22°C, and food and water *ad libitum*. We developed a syngeneic and orthotopic mouse mammary cancer model in female BALB/cJ immunocompetent mice. To do so, 4T1-luciferase-expressing mouse mammary cancer cells were injected into the fifth mammary fat pad of 6 weeks-old mice. The luciferase activity was mainly used to follow secondary tumour appearance and growth *in vivo*, subsequent to D-luciferin (150 mg/kg) intraperitoneal injection and bioluminescent imaging (IVIS Lumina II, Perkin Elmer). Primary tumour volume (mm^3) and growth over time were most effectively measured with a calliper, twice a week, and calculated as (L

569 x l²)/2 (in mm). Metastases were counted macroscopically at the completion of studies, during
570 autopsies. Animal weight was measured once a week.
571 In experiments comparing the role of the number of injected cells on primary tumour growth, in
572 mice expressing the *P2rx7* gene or not, cell suspensions of either $1x10^6$ or $1x10^4$ 4T1-luc derived
573 CTL (P2X7 +) cancer cells were injected to BALB/cJ mice *P2rx7* -/- (Generous gift of Prof. Niklas
574 Rye Jørgensen, Department of Clinical Biochemistry, Rigshospitalet, Glostrup, Denmark) or to
575 BALB/cJ *P2rx7* +/+ litter mate control mice, which were housed in the same environmentally
576 controlled conditions. *P2rx7* -/- mice [101] were backcrossed onto the BALB/cJ background as
577 previously described [74].
578 In experiments assessing the effect of *P2rx7* gene expression in mammary cancer cells on primary
579 tumour growth and metastatic progression, $1x10^4$ CTL ($P2rx7^{+/+}$), Crispr#1 or Crispr#2 ($P2rx7^{-/-}$)
580 4T1-derived mammary cancer-cells (see section "***Cells and cell culture")*** in 100 µL of a PBS
581 solution were injected in the mammary fat pad, under isoflurane anaesthesia, of wild-type BALB/cJ
582 mice (Janvier Labs, Saint Berthevin, France).
583 In experiments assessing the efficacy of P2X7 antagonism, $1x10^4$ CTL ($P2rx7^{+/+}$) cells were
584 injected in the mammary fat pad of wild-type BALB/cJ mice (Janvier Labs, Saint Berthevin,
585 France), and treatments have been randomly administrated once tumours reached 80 mm^3. Then,
586 230 µl of 3 mg/ml A437079 solution or 100 µl of a 300 nM AZ10606120 solution were injected
587 intraperitoneally every two days. Primary tumours were fixed in formalin, included in paraffin, and
588 cut in 5-µm tissue sections. Slides were deparaffinized, rehydrated, and heated in citrate buffer pH 6
589 for antigenic retrieval. Immunohistochemistry was performed using primary antibody anti-P2X7
590 (APR-008 Alomone, Israel) and the streptavidin-biotin-peroxidase method with diaminobenzidine
591 as the chromogen (Kit LSAB, Dakocytomation). Slides were finally counterstained with
592 haematoxylin. Negative controls were obtained by omission of the primary antibody or incubation
593 with an irrelevant antibody.

Mathematical model for assessing mammary tumour growth depending on treatments – A Gompertz model was used to describe mammary tumour growth over time. This model included three parameters, *i.e.* the first-order growth rate constant (kgrowth), the maximum tumour volume (Vmax) and the power coefficient γ. In addition, the effect of treatment (EFF) on tumour volume was estimated as a parameter being 0 without treatment (*i.e.* before treatment, in both A438079 and AZ10606120 groups, and every time in the vehicle group) and estimated when treatment was administered. Model parameters were estimated using nonlinear mixed-effects modelling. This approach allows describing the inter-subject variability in the population (mean and inter-subject standard deviations) and quantifying the association of factors of variability (referred as being « covariates ») with inter-subject distribution of Gomperz parameters. The influence of treatment condition (A438079 or AZ10606120) was tested as a covariate on both kgrowth and Vmax. This analysis was carried out using MonolixSuite2018 (Lixoft®, Antony, France). The effect of treatment and treatment condition on each parameter was tested using likelihood ratio test (LRT).

Data presentation and statistical analysis **-** Data are displayed as median ± range (n = number of cells/ independent experiments). One-way ANOVA followed by a Dunn's Multiple Comparison Test, Wilcoxon Signed Rank Test and Mann-Whitney rank sum test were used to compare different conditions, as indicated in the figure legends. Statistical significance is indicated as: *, $p < 0.05$; **, $p < 0.01$ and ***, $p < 0.001$. NS stands for not statistically different.

Data availability –The authors declare that all other data supporting the findings of this study are available within the paper and its supplementary information files or available from the authors upon request.

References

1 North, R. A. Molecular physiology of P2X receptors. *Physiol Rev* **82**, 1013-1067 (2002).

2 Surprenant, A., Rassendren, F., Kawashima, E., North, R. A. & Buell, G. The cytolytic P2Z receptor for extracellular ATP identified as a P2X receptor (P2X7). *Science* **272**, 735-738 (1996).

3 Jiang, L. H., Baldwin, J. M., Roger, S. & Baldwin, S. A. Insights into the Molecular Mechanisms Underlying Mammalian P2X7 Receptor Functions and Contributions in Diseases, Revealed by Structural Modeling and Single Nucleotide Polymorphisms. *Front Pharmacol* **4**, 55 (2013).

4 North, R. A. & Surprenant, A. Pharmacology of cloned P2X receptors. *Annu Rev Pharmacol Toxicol* **40**, 563-580 (2000).

5 Roger, S., Gillet, L., Baroja-Mazo, A., Surprenant, A. & Pelegrin, P. C-terminal calmodulin-binding motif differentially controls human and rat P2X7 receptor current facilitation. *J Biol Chem* **285**, 17514-17524 (2010).

6 Roger, S., Pelegrin, P. & Surprenant, A. Facilitation of P2X7 receptor currents and membrane blebbing via constitutive and dynamic calmodulin binding. *J Neurosci* **28**, 6393-6401 (2008).

7 Yan, Z. *et al.* Experimental characterization and mathematical modeling of P2X7 receptor channel gating. *J Neurosci* **30**, 14213-14224 (2010).

8 Surprenant, A. & North, R. A. Signaling at purinergic P2X receptors. *Annu Rev Physiol* **71**, 333-359 (2009).

9 Di Virgilio, F., Dal Ben, D., Sarti, A. C., Giuliani, A. L. & Falzoni, S. The P2X7 Receptor in Infection and Inflammation. *Immunity* **47**, 15-31, doi:10.1016/j.immuni.2017.06.020 (2017).

10 McLarnon, J. G. Roles of purinergic P2X7 receptor in glioma and microglia in brain tumors. *Cancer Lett* **402**, 93-99, doi:10.1016/j.canlet.2017.05.004 (2017).

11 Bergamin, L. S. *et al.* Role of the P2X7 receptor in in vitro and in vivo glioma tumor growth. *Oncotarget* **10**, 4840-4856, doi:10.18632/oncotarget.27106 (2019).

12 Filippin, K. J. *et al.* Involvement of P2 receptors in hematopoiesis and hematopoietic disorders, and as pharmacological targets. *Purinergic Signal*, doi:10.1007/s11302-019-09684-z (2019).

13 Roger, S. *et al.* Understanding the roles of the P2X7 receptor in solid tumour progression and therapeutic perspectives. *Biochim Biophys Acta* **1848**, 2584-2602, doi:10.1016/j.bbamem.2014.10.029 (2015).

14 Li, X. *et al.* Decreased expression of P2X7 in endometrial epithelial pre-cancerous and cancer cells. *Gynecol Oncol* **106**, 233-243 (2007).

15 Li, X. *et al.* P2X(7) receptor expression is decreased in epithelial cancer cells of ectodermal, uro-genital sinus, and distal paramesonephric duct origin. *Purinergic Signal* **5**, 351-368 (2009).

16 Adinolfi, E. *et al.* Expression of the P2X7 receptor increases the Ca2+ content of the endoplasmic reticulum, activates NFATc1, and protects from apoptosis. *J Biol Chem* **284**, 10120-10128 (2009).

17 Adinolfi, E. *et al.* Trophic activity of a naturally occurring truncated isoform of the P2X7 receptor. *Faseb J* (2010).

18 Adinolfi, E. *et al.* Expression of P2X7 Receptor Increases In Vivo Tumor Growth. *Cancer Res* **72**, 2957-2969 (2012).

19 Takai, E., Tsukimoto, M., Harada, H. & Kojima, S. Autocrine signaling via release of ATP and activation of P2X7 receptor influences motile activity of human lung cancer cells. *Purinergic Signal* (2014).

20 Jelassi, B. *et al.* Anthraquinone emodin inhibits human cancer cell invasiveness by antagonizing P2X7 receptors. *Carcinogenesis* **34**, 1487-1496 (2013).
21 Jelassi, B. *et al.* P2X(7) receptor activation enhances SK3 channels- and cystein cathepsin-dependent cancer cells invasiveness. *Oncogene* **30**, 2108-2122 (2011).
22 Giannuzzo, A., Pedersen, S. F. & Novak, I. The P2X7 receptor regulates cell survival, migration and invasion of pancreatic ductal adenocarcinoma cells. *Mol Cancer* **14**, 203, doi:10.1186/s12943-015-0472-4 (2015).
23 Giannuzzo, A. *et al.* Targeting of the P2X7 receptor in pancreatic cancer and stellate cells. *Int J Cancer* **139**, 2540-2552, doi:10.1002/ijc.30380 (2016).
24 Qiu, Y. *et al.* P2X7 mediates ATP-driven invasiveness in prostate cancer cells. *PLoS One* **9**, e114371, doi:10.1371/journal.pone.0114371 (2014).
25 Roger, S. & Pelegrin, P. P2X7 receptor antagonism in the treatment of cancers. *Expert Opin Investig Drugs* **20**, 875-880 (2011).
26 Greig, A. V. *et al.* Expression of purinergic receptors in non-melanoma skin cancers and their functional roles in A431 cells. *J Invest Dermatol* **121**, 315-327 (2003).
27 Coutinho-Silva, R. *et al.* P2X and P2Y purinergic receptors on human intestinal epithelial carcinoma cells: effects of extracellular nucleotides on apoptosis and cell proliferation. *Am J Physiol Gastrointest Liver Physiol* **288**, G1024-1035 (2005).
28 Feng, Y. H., Li, X., Wang, L., Zhou, L. & Gorodeski, G. I. A truncated P2X7 receptor variant (P2X7-j) endogenously expressed in cervical cancer cells antagonizes the full-length P2X7 receptor through hetero-oligomerization. *J Biol Chem* **281**, 17228-17237 (2006).
29 Aymeric, L. *et al.* Tumor cell death and ATP release prime dendritic cells and efficient anticancer immunity. *Cancer Res* **70**, 855-858 (2010).
30 Ghiringhelli, F. *et al.* Activation of the NLRP3 inflammasome in dendritic cells induces IL-1beta-dependent adaptive immunity against tumors. *Nat Med* **15**, 1170-1178 (2009).
31 De Marchi, E. *et al.* The P2X7 receptor modulates immune cells infiltration, ectonucleotidases expression and extracellular ATP levels in the tumor microenvironment. *Oncogene* **38**, 3636-3650, doi:10.1038/s41388-019-0684-y (2019).
32 Adinolfi, E., De Marchi, E., Orioli, E., Pegoraro, A. & Di Virgilio, F. Role of the P2X7 receptor in tumor-associated inflammation. *Curr Opin Pharmacol* **47**, 59-64, doi:10.1016/j.coph.2019.02.012 (2019).
33 Slater, M., Danieletto, S. & Barden, J. A. Expression of the apoptotic calcium channel P2X7 in the glandular epithelium. *J Mol Histol* **36**, 159-165 (2005).
34 Park, M. *et al.* Involvement of the P2X7 receptor in the migration and metastasis of tamoxifen-resistant breast cancer: effects on small extracellular vesicles production. *Scientific reports* **9**, 11587, doi:10.1038/s41598-019-47734-z (2019).
35 Xia, J., Yu, X., Tang, L., Li, G. & He, T. P2X7 receptor stimulates breast cancer cell invasion and migration via the AKT pathway. *Oncol Rep* **34**, 103-110, doi:10.3892/or.2015.3979 (2015).
36 Brisson, L., Reshkin, S. J., Gore, J. & Roger, S. pH regulators in invadosomal functioning: Proton delivery for matrix tasting. *Eur J Cell Biol* **91**, 847-860 (2012).
37 Aslakson, C. J. & Miller, F. R. Selective events in the metastatic process defined by analysis of the sequential dissemination of subpopulations of a mouse mammary tumor. *Cancer Res* **52**, 1399-1405 (1992).
38 Nelson, D. W. *et al.* Structure-activity relationship studies on a series of novel, substituted 1-benzyl-5-phenyltetrazole P2X7 antagonists. *J Med Chem* **49**, 3659-3666 (2006).
39 Allsopp, R. C., Dayl, S., Schmid, R. & Evans, R. J. Unique residues in the ATP gated human P2X7 receptor define a novel allosteric binding pocket for the selective antagonist AZ10606120. *Scientific reports* **7**, 725, doi:10.1038/s41598-017-00732-5 (2017).
40 Khalid, M. *et al.* Carcinoma-specific expression of P2Y11 receptor and its contribution in ATP-induced purinergic signalling and cell migration in human hepatocellular carcinoma cells. *Oncotarget* **8**, 37278-37290, doi:10.18632/oncotarget.16191 (2017).

41 Chadet, S. *et al.* Hypoxia/Reoxygenation Inhibits P2Y11 Receptor Expression and Its Immunosuppressive Activity in Human Dendritic Cells. *J Immunol* **195**, 651-660, doi:10.4049/jimmunol.1500197 (2015).

42 Linder, S. Invadosomes at a glance. *J Cell Sci* **122**, 3009-3013 (2009).

43 Brisson, L. *et al.* NaV1.5 Na+ channels allosterically regulate the NHE-1 exchanger and promote the activity of breast cancer cell invadopodia. *J Cell Sci* **126**, 4835-4842 (2013).

44 Linder, S., Wiesner, C. & Himmel, M. Degrading devices: invadosomes in proteolytic cell invasion. *Annu Rev Cell Dev Biol* **27**, 185-211 (2011).

45 Sanz-Moreno, V. *et al.* Rac activation and inactivation control plasticity of tumor cell movement. *Cell* **135**, 510-523, doi:10.1016/j.cell.2008.09.043 (2008).

46 Sahai, E. & Marshall, C. J. Differing modes of tumour cell invasion have distinct requirements for Rho/ROCK signalling and extracellular proteolysis. *Nat Cell Biol* **5**, 711-719, doi:10.1038/ncb1019 (2003).

47 Maldonado, M. D. M. & Dharmawardhane, S. Targeting Rac and Cdc42 GTPases in Cancer. *Cancer Res* **78**, 3101-3111, doi:10.1158/0008-5472.CAN-18-0619 (2018).

48 Parkin, D. M., Bray, F., Ferlay, J. & Pisani, P. Global cancer statistics, 2002. *CA Cancer J Clin* **55**, 74-108 (2005).

49 Clark, A. G. & Vignjevic, D. M. Modes of cancer cell invasion and the role of the microenvironment. *Curr Opin Cell Biol* **36**, 13-22, doi:10.1016/j.ceb.2015.06.004 (2015).

50 Mierke, C. T. The matrix environmental and cell mechanical properties regulate cell migration and contribute to the invasive phenotype of cancer cells. *Reports on progress in physics. Physical Society* **82**, 064602, doi:10.1088/1361-6633/ab1628 (2019).

51 Pandya, P., Orgaz, J. L. & Sanz-Moreno, V. Modes of invasion during tumour dissemination. *Molecular oncology* **11**, 5-27, doi:10.1002/1878-0261.12019 (2017).

52 Bon, E. *et al.* SCN4B acts as a metastasis-suppressor gene preventing hyperactivation of cell migration in breast cancer. *Nature communications* **7**, 13648, doi:10.1038/ncomms13648 (2016).

53 Di Virgilio, F., Sarti, A. C., Falzoni, S., De Marchi, E. & Adinolfi, E. Extracellular ATP and P2 purinergic signalling in the tumour microenvironment. *Nat Rev Cancer* **18**, 601-618, doi:10.1038/s41568-018-0037-0 (2018).

54 Pellegatti, P. *et al.* Increased level of extracellular ATP at tumor sites: in vivo imaging with plasma membrane luciferase. *PLoS One* **3**, e2599 (2008).

55 Raffaghello, L., Chiozzi, P., Falzoni, S., Di Virgilio, F. & Pistoia, V. The P2X7 receptor sustains the growth of human neuroblastoma cells through a substance P-dependent mechanism. *Cancer Res* **66**, 907-914 (2006).

56 Di Virgilio, F. *et al.* Cytolytic P2X purinoceptors. *Cell Death Differ* **5**, 191-199 (1998).

57 Slater, M., Danieletto, S., Gidley-Baird, A., Teh, L. C. & Barden, J. A. Early prostate cancer detected using expression of non-functional cytolytic P2X7 receptors. *Histopathology* **44**, 206-215 (2004).

58 Slater, M., Scolyer, R. A., Gidley-Baird, A., Thompson, J. F. & Barden, J. A. Increased expression of apoptotic markers in melanoma. *Melanoma Res* **13**, 137-145 (2003).

59 Gorodeski, G. I. P2X7-mediated chemoprevention of epithelial cancers. *Expert Opin Ther Targets* **13**, 1313-1332 (2009).

60 Adinolfi, E. *et al.* Basal activation of the P2X7 ATP receptor elevates mitochondrial calcium and potential, increases cellular ATP levels, and promotes serum-independent growth. *Mol Biol Cell* **16**, 3260-3272 (2005).

61 Bours, M. J., Swennen, E. L., Di Virgilio, F., Cronstein, B. N. & Dagnelie, P. C. Adenosine 5'-triphosphate and adenosine as endogenous signaling molecules in immunity and inflammation. *Pharmacol Ther* **112**, 358-404 (2006).

62 Adinolfi, E. *et al.* Accelerated tumor progression in mice lacking the ATP receptor P2X7. *Cancer Res* **75**, 635-644, doi:10.1158/0008-5472.CAN-14-1259 (2015).

63 Hofman, P. *et al.* Genetic and pharmacological inactivation of the purinergic P2RX7 receptor dampens inflammation but increases tumor incidence in a mouse model of colitis-associated cancer. *Cancer Res* **75**, 835-845, doi:10.1158/0008-5472.CAN-14-1778 (2015).
64 Holzel, M. & Tuting, T. Inflammation-Induced Plasticity in Melanoma Therapy and Metastasis. *Trends Immunol* **37**, 364-374, doi:10.1016/j.it.2016.03.009 (2016).
65 Janakiram, N. B. & Rao, C. V. The role of inflammation in colon cancer. *Adv Exp Med Biol* **816**, 25-52, doi:10.1007/978-3-0348-0837-8_2 (2014).
66 Zhang, Y., Cheng, H., Li, W., Wu, H. & Yang, Y. Highly-expressed P2X7 receptor promotes growth and metastasis of human HOS/MNNG osteosarcoma cells via PI3K/Akt/GSK3beta/beta-catenin and mTOR/HIF1alpha/VEGF signaling. *Int J Cancer* **145**, 1068-1082, doi:10.1002/ijc.32207 (2019).
67 Lou, Y. *et al.* Epithelial-mesenchymal transition (EMT) is not sufficient for spontaneous murine breast cancer metastasis. *Developmental dynamics : an official publication of the American Association of Anatomists* **237**, 2755-2768, doi:10.1002/dvdy.21658 (2008).
68 Saitoh, M. Involvement of partial EMT in cancer progression. *Journal of biochemistry* **164**, 257-264, doi:10.1093/jb/mvy047 (2018).
69 Guo, Q., Betts, C., Pennock, N., Mitchell, E. & Schedin, P. Mammary Gland Involution Provides a Unique Model to Study the TGF-beta Cancer Paradox. *Journal of clinical medicine* **6**, doi:10.3390/jcm6010010 (2017).
70 Driffort, V. *et al.* Ranolazine inhibits NaV1.5-mediated breast cancer cell invasiveness and lung colonization. *Mol Cancer* **13**, 264, doi:10.1186/1476-4598-13-264 (2014).
71 Csolle, C. *et al.* Neurochemical Changes in the Mouse Hippocampus Underlying the Antidepressant Effect of Genetic Deletion of P2X7 Receptors. *PLoS One* **8**, e66547, doi:10.1371/journal.pone.0066547 (2013).
72 Le Gall, S. M. *et al.* Loss of P2X7 receptor plasma membrane expression and function in pathogenic B220+ double-negative T lymphocytes of autoimmune MRL/lpr mice. *PLoS One* **7**, e52161, doi:10.1371/journal.pone.0052161 (2012).
73 Barry, D. J., Durkin, C. H., Abella, J. V. & Way, M. Open source software for quantification of cell migration, protrusions, and fluorescence intensities. *J Cell Biol* **209**, 163-180, doi:10.1083/jcb.201501081 (2015).
74 Syberg, S. *et al.* Genetic Background Strongly Influences the Bone Phenotype of P2X7 Receptor Knockout Mice. *J Osteoporos* **2012**, 391097, doi:10.1155/2012/391097 (2012).

Acknowledgements

This work was supported by the "Ministère de la Recherche et des Technologies", the "Ligue Nationale Contre le Cancer – Interrégion Grand-Ouest" to SR, the Région Centre-Val de Loire (grant "CancerInflam n-3" to SR), the "Association CANCEN". S.R. was recipient of a prize "Prix Ruban Rose Avenir 2017" from the Charity "le Cancer du sein: parlons-en!". L-HJ was recipient of an Invited Professorship of the University of Tours. LB was recipient of a Post-doctoral grant from the Région Centre-Val de Loire, a Prestige Incoming mobility fellowship (Campus France, FP7 funded research, EU), and of a Prize from "Fondation Tourre" (France).

We thank Ms Catherine Le Roy and Mrs Carole Desplanches for secretary and administrative assistance, and Ms Isabelle Domingo for cell culture assistance. We thank Ms Roseline Guibon and Prof Gaelle Fromont for the assistance with immunohistochemistry. We thank Mrs Stéphanie Rétif and Mrs Marilyne Le Mée for the assistance with *in vivo* experiments performed at CNRS UPS44 CIPA, Orléans. We thank Prof. Laurent Counillon (CNRS UMR7370, University of Nice-Sophia Antipolis, France) for the generous gift of the LifeAct plasmid and Prof. Niklas Rye Jørgensen (Department of Clinical Biochemistry, Rigshospitalet, Glostrup, Denmark) for the generous gift of BALB/cJ *P2rx7* $^{+}/^{-}$ mice.

Author contributions

All authors contributed extensively to the work presented in this study. L.B. performed and analysed immunofluorescence imaging, time-lapse microscopy experiments, assessed cell adhesion and Calcium imaging. L.B., S.Cha., B.J., J.C. performed cell culture, molecular and cellular biology experiments, assessed cell viability, migration and invasion. S.R and B.J. performed electrophysiology experiments. S.L., A.L.P., I.C., A.G. performed *in vivo* mice experiments. D.T. performed mathematical model for the assessment of mammary tumour growth. L.B., P.B. L.-H.J.

and S.R. analysed *in vivo* data. S.C. contributed in discussion and revision of the manuscript. S.R., F.T. and L.-H.J obtained research grants. S.R, P.B and L.-H.J. directed the research, designed the study, analysed the data and wrote the manuscript.

Competing financial interest

The authors declare no competing financial interests.

Correspondence and requests for materials should be addressed to S.R. (sebastien.roger@univ-tours.fr)

839 **Figure legends**

840

841 **Figure 1: P2X7 receptor is functional in mammary cancer cells and drives 2- and 3-**
842 **dimensions invasiveness. a,** P2X1-7 mRNA expression (expression of *P2rx1-P2rx7* genes) was
843 analysed by conventional RT-PCR after 30 amplification cycles from 4T1 mouse mammary cancer
844 cells. **b**, Representative whole-cell patch clamp recordings of ATP-induced currents from 4T1
845 mouse mammary cancer cells. Membrane potential was held at -60 mV. While 10-s application of
846 10 μM ATP (left recording) was not able to produce any current, the application of 5 mM ATP
847 (right recording) produced a non-desensitizing P2X7-like inward current that was reduced by the
848 use of 10 μM A438079 antagonist. **c**, Left side : representative inward currents recorded from one
849 4T1 cell, in response to 10 s-long applications of increasing concentrations of ATP (0.3, 1, 3, 5 and
850 10 mM). Right side: the ATP dose-response curve for inward currents, expressed as a ratio of the
851 maximum current obtained with 10 mM ATP. The EC_{50} obtained from a sigmoidal fit and the Hill
852 equation was 4.3 ± 0.2 mM (n = 5-6 cells). **d**, Intracellular levels of free Ca^{2+} were monitored by the
853 use of Fura2 fluorescence expressed as a ratio of the 510 nm produced by excitations at 340 nm and
854 380 nm wavelengths, after 300 μM BzATP agonist stimulation, in the absence (black traces,
855 control) or presence (red traces) of P2X7 antagonist A438079 (10 μM). This same protocol was
856 performed in the presence of 3 mM extracellular Ca^{2+} (left traces) or in the absence of extracellular
857 Ca^{2+} (right traces). These data are averaged from 4 independent experiments. There is a statistically
858 significant difference in BzATP-induced Ca^{2+} responses in the presence of 3 mM extracellular Ca^{2+}
859 at $p < 0.001$ using two-way ANOVA, but no significant difference in the absence of extracellular
860 Ca^{2+}. **e**, Similar protocol as in d, using AZ10606120 (300 nM) as another P2X7 antagonist (blue
861 traces) as compared to the control condition (vehicle, black traces), in the presence of 3 mM
862 extracellular Ca^{2+} (left traces) or in the absence of extracellular Ca^{2+} (right traces). These data are
863 averaged from 3 independent experiments. There is a statistically significant difference in BzATP-
864 induced Ca^{2+} responses in the presence of 3 mM extracellular Ca^{2+} at $p < 0.001$ using two-way

ANOVA, but no significant difference in the absence of extracellular Ca^{2+}. **f**, 4T1 cell viability over 24 h in the presence of increasing concentrations of ATP (from 0.03 to 3 mM), in the absence or presence of 10 μM A438079, and expressed relatively to the control condition (vehicle). Results are from 4 independent experiments. There is a statistically significant difference when comparing each of the two treatment groups to the control condition at *$p<0.05$, **$p<0.01$ and ***$p<0.0001$, but there was no significant difference between the ATP treatment and the ATP+A438079 treatment, using t-test. **g**, 4T1 cell viability over 24h in the presence of increasing concentrations of BzATP (from 0.01 to 1 mM), expressed relatively to the control condition (vehicle). Results are from 4 independent experiments. There was no significant difference between the BzATP treatment and control condition. **h**, 4T1 2D-cell invasiveness was assessed over 24 h using trans-well invasion inserts in the absence or presence of BzATP (300 μM), in cells transfected with a null-target siRNA (siCTL) or a specific siRNA targeting *P2rx7* expression (siP2X7). Results are from 6 independent experiments and expressed relatively to the siCTL condition, in the absence of BzATP stimulation (CTL). ** indicates a statistically significant difference at $p<0.01$ when comparing siCTL/BzATP to siCTL/CTL, using Mann-Whitney Rank Sum Test. **i**, 4T1 2D-cell invasiveness was assessed over 24 h using trans-well invasion inserts in the absence or presence of BzATP (300 μM), and in the absence or presence of P2X7 antagonist A438079 (10 μM). Results are from 4-6 independent experiments and are expressed relatively to the control condition (CTL), in the absence of BzATP and of A438079. * indicates a statistically significant difference at $p<0.05$ when comparing BzATP treatment to CTL, using Wilcoxon Signed Rank Test. **j**, 4T1 3D-cell invasiveness was assessed over 72 h. Image on the left show the morphology of cancer cell spheroids that was assessed before (T = 0 h) or after 72 h treatment (T = 72 h) in control condition (vehicle) or with BzATP (300 μM) in the absence or presence of A438079 (10 μM). Scale bar, 100 μm. On the right side is the summary of assessment of the spheroid circularity from 14-20 independent experiments. * indicates a statistically significant difference at $p<0.05$ using Dunn's Multiple Comparison Test.

Figure 2: P2X7 receptor promotes invadopodial activity of extracellular matrix degradation. **a,** 4T1 mouse mammary and MDA-MB-435s human cancer cells were grown on Matrigel™ containing DQ-BSA as a fluorogenic substrate for proteases, emitting red fluorescence when degraded. P2X7 receptor was immunodetected using a rabbit primary antibody against P2X7 protein and a secondary ant-rabbit IgG antibody conjugated to AF488. The right panel shows the fluorescence values for the two channels at the locations indicated by a blue arrow. Scale bar, 100 μm. **b**, Invadopodia entrapped into a 2%-gelatin matrix were fractionated and separated from cytosol and membranes-enriched fractions. The quality of the fractions was assessed by western blotting after SDS-PAGE, using cytosolic (HSC70), membrane (caveolin-1, β-adaptin) and invadopodia (cathepsin B, cortactin, focal adhesion kinase) markers. P2X7 proteins were found to be present in the membrane fractions and enriched in the invadopodia fraction. This figure is representative of 5 independent experiments. **c**, The invadopodial activity was assessed as being F-actin foci (green labelling, phalloidin-488) co-localised with focused proteolytic activities (red labelling, DQ-BSA proteolysis) from 4T1 cells grown for 24 h on Matrigel™ containing DQ-BSA in control condition (vehicle), or stimulated with 300 μM BzATP, in the presence and absence of 10 μM A438079. "Coloc" indicates co-localization of degradative activity and F-actin foci, and appears as white pixels. Scale bar, 50 μm. **d**, The number of degradation areas per cell was counted in 20 images, from 5 independent experiments. * indicates a statistically significant difference at $p<0.05$ using Dunn's Multiple Comparison Test. **e**, The number of invadopodia (identified as being F-actin foci colocalized with matrix degradation spots) was counted per cell in the same experiments as in d. There was no significant difference among the four treatment conditions.

Figure 3: P2X7 receptor stimulation promotes the acquisition of a mesenchymal phenotype. a, F-actin cytoskeleton was visualized using phalloidin-488 in 4T1 cells stimulated with 300 μM BzATP at the time indicated. Rapid morphological changes appear as rapidly as after 6 min stimulation. Scale bar, 25 μm. **b**, The number of new filopodia per cell was counted per hour in

cells transfected with the LifeAct plasmid and studied in the presence of 300 µM BzATP, in the presence or absence of 10 µM A438079. * indicates a statistically significant difference at $p<0.05$ using Dunnett's Multiple Comparison Test. **c**, The velocity of filopodia to form and extend (in µm/min) was measured in the same experiments as in **b**. There was no significant difference among the four experimental groups. **d**, On the left side, representative western blots show total and active GTP-bound forms of Cdc42, RhoA, and Rac1 pulled down by GST-RBD in 4T1 cells in control conditions or stimulated with 300 µM BzATP, in the presence and absence of 10 µM A438079. His-tagged proteins are used as positive controls for the quality of the pull-down experiment. On the right side, graphs show quantifications of GTP-bound RhoGTPases (active form), normalized to total protein level, and expressed relatively to that of the control condition (vehicle). Results are from 4-7 independent experiments. * indicates statistically significant difference at $p<0.05$, using Mann-Whitney rank sum test. **e**, mRNA expression levels of *P2rx7*, *SNAI1*, *ZEB1*, *TWIST1*, *ZO1* and *CDH1* assessed by RT-qPCR in 4T1 cells stimulated by 300 µM BzATP for 24 h and expressed relatively to the GUSB reference gene and as ratios to the expression levels in control condition without BzATP (n = 9-11 independent experiments). SNAI1 was significantly higher, and ZO1 was significantly lower after BzATP treatment compared to control condition at *, $p<0.05$, using Mann-Whitney rank sum test.

Figure 4: P2X7 receptor in mammary cancer cells enhances primary tumour growth and metastatic development *in vivo*. a, *P2rx7* mRNA expression levels assessed by RT-qPCR in CTL, Crispr#1 and Crispr#2 cell lines, expressed relatively to 4T1 cells. * indicated a statistically significant difference from CTL cells at $p<0.05$ using Mann-Whitney Rank sum test. **b,** 2-D cancer cell invasiveness of CTL**,** Crispr#1 and Crispr#2 cell lines, in the absence or presence of 300 µM BzATP, expressed relatively to the CTL cell line without BzATP (n = 5-8 independent experiments). * indicates a statistically significant difference from CTL/no BzATP condition at $p<0.05$, ¤ indicates a statistically significant difference from CTL/BzATP at $p<0.05$, using Dunn's

Multiple Comparison Test. NS, stands for no statistically significant difference. **c**, Cell proliferation over 4 days of CTL, Crispr#1 and Crispr#2 cell lines in the absence of 300 µM BzATP, expressed relatively to the CTL condition. Results are from 6-10 independent experiments. * indicates a statistically significant difference from CTL at $p<0.05$ using Dunn's Multiple Comparison Test. **d,** Cell adhesion of CTL, Crispr#1 and Crispr#2 clones, expressed relatively to CTL. Results are from 10 independent experiments. * indicates a statistically significant difference from CTL at $p<0.05$ using Dunn's Multiple Comparison Test. **e-i**, *In vivo* mouse experiments testing the effect of *P2rx7* gene expression in host mice on primary tumour growth and metastasis development, with two numbers of cancer cells implanted. **e**, Top, cartoon describing the experimental procedure, in which CTL cells, derived from 4T1-Luc expressing *P2rx7* gene, were implanted to the fifth mammary fat pad of 6 weeks-old female wild-type BALB/cJ (*P2rx7*$^{+/+}$) *or* P2X7 knock-out BALB/cJ *(P2rx7*$^{-/-}$) mice. Bottom, representative bioluminescent images of a wild-type mouse, on 14 and 35 days after cell implantation, identifying primary tumours as well as metastatic foci. **f**, Primary mammary tumour growth in wild-type BALB/cJ (*P2rx7*$^{+/+}$, n = 8) *or* P2X7 knock-out BALB/cJ *(P2rx7*$^{-/-}$, n = 8) mice as a function of time following the implantation of $1x10^6$ CTL cells on day 0. **g**, Analysis of the number of metastases per mouse, identified at necropsy, in the experiment described in f. NS stands for no statistical significant difference. **h**, Primary mammary tumour growth in wild-type BALB/cJ (*P2rx7*$^{+/+}$, n = 8) or P2X7 knock-out BALB/cJ (*P2rx7*$^{-/-}$, n = 8) mice as a function of time following the implantation of $1x10^4$ CTL cells on day 0. **i**, Analysis of the number of metastases per mouse, identified at necropsy, in the experiment described in h. NS stands for no statistically significant difference. **j-l**, *In vivo* mouse experiments assessing the role of *P2rx7* gene expression in mammary cancer cells on primary tumour growth and metastasis development. **j**, Cartoon describing the experimental procedure, in which CTL (*P2rx7*$^{+/+}$*)*, Crispr#1 or Crispr#2 (both knock-down for the *P2rx7* expression) cells were implanted to the fifth mammary fat pad of 6 weeks-old female wild-type BALB/cJ (*P2rx7*$^{+/+}$) at a density of $1x10^4$ CTL cells per mouse (8 mice per group). **k**, Primary mammary tumour growth in wild-type BALB/cJ (*P2rx7*$^{+/+}$) as a function of time

following the implantation of CTL, Crispr#1 or Crispr#2 cells on day 0. *** indicates a statistically significant difference from the CTL group at $p<0.001$ using two-way ANOVA. **l**, Analysis of the number of metastases per mouse, in the three experimental groups, identified at necropsy, in the experiment described in j. * indicates a statistically significant difference from the CTL group at $p<0.05$ using Dunn's Multiple Comparison test.

Figure 5: P2X7 antagonism slows mammary tumour growth. a, *In vivo* mouse experiments assessing the effects of treatments with two P2X7 antagonist (A438079 or AZ10606120) on primary tumour growth, in which cancer cells and host organisms both express the *P2rx7* gene. **b**, primary mammary tumour growth represented as a function of the duration of the treatment depending on antagonist treatments (A438079 or AZ10606120) compared to the injection of vehicle. **c-e,** A, Gompertz model was used to assess mammary tumour growth as a function of time for **c**, vehicle group, **d**, A438079 and **e**, AZ10606120. Black, red and blue dots represent individual tumour volumes of these respective categories, blue areas are 90% model prediction intervals and lines are the median tumour growth. Estimated mean (inter-individual standard deviation) of model parameters were kgrowth = 0.64 day-1 (39%), Vmax = 1,620 mm^3 (64%), EFF = 0.52 (82%) and γ = 0.17 (–). This analysis showed that tumour volume doubled in a mean time of 0.64 day, that the mean maximum tumour volume was 1,620 mm^3 and that tumour growth was twice slower in the presence of A438079 or AZ10606120 treatment ($p<10^{-10}$) as compared to the vehicle group. There was no difference in the efficacy of these two treatments ($p = 0.08$). **f**, Assessment of the number of metastases per mouse, in the three experimental groups; vehicle, A438079 and AZ10606120. There was no statistical difference. **g**, Percent survival curve in the three experimental group indicating a significant prolonged survival of mice treated with AZ10606120 at $p = 0.0464$ using Gehan-Breslow-Wilcoxon Test.

995

996

997

998

999

Figure 1

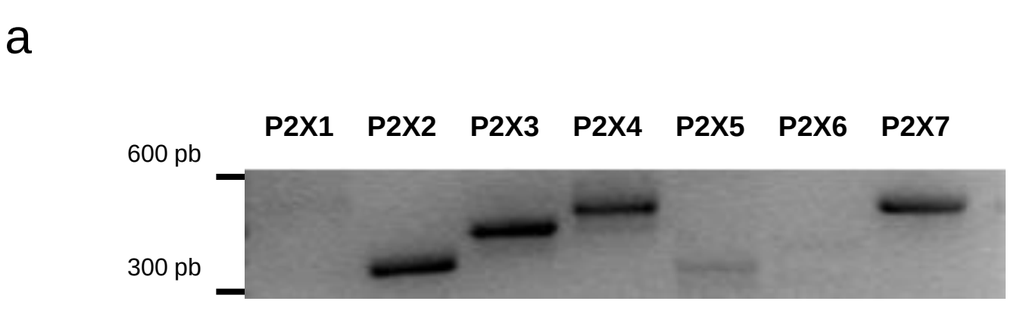
a
P2X1
P2X2
P2X3
P2X4
P2X5
P2X6
P2X7
600 pb
300 pb

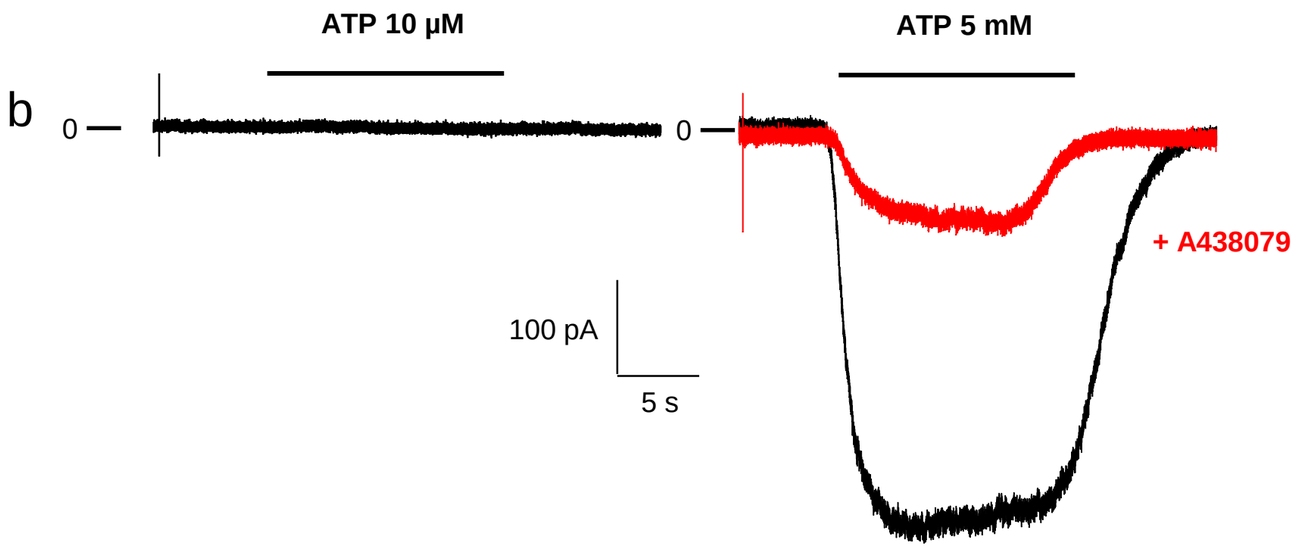
b
ATP 10 µM
ATP 5 mM
0
0
+ A438079
100 pA
5 s

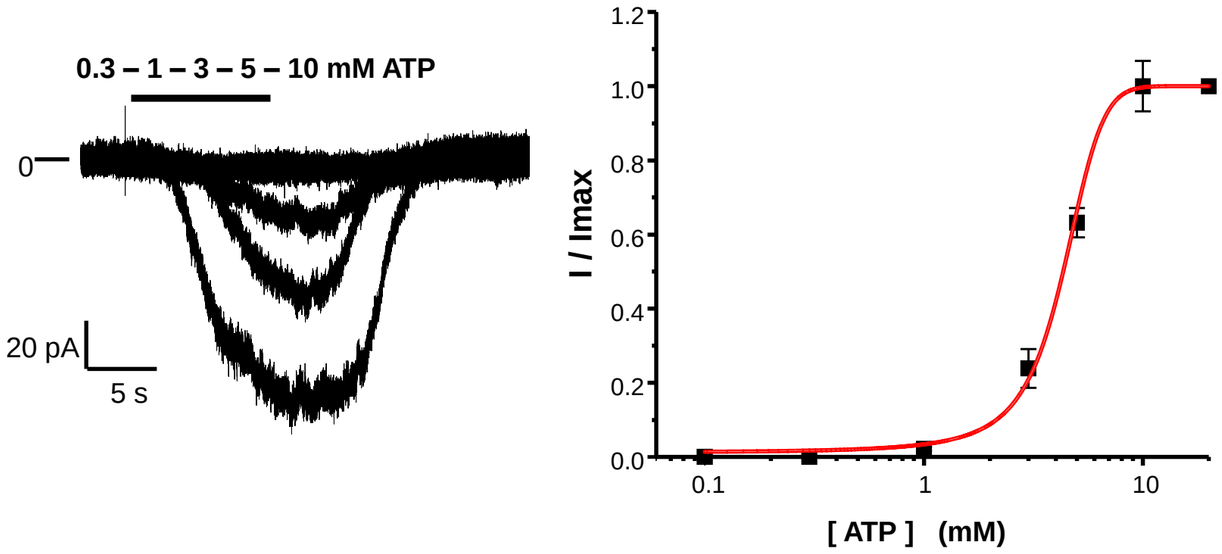
c
0.3 – 1 – 3 – 5 – 10 mM ATP
0
20 pA
5 s
I / Imax
[ATP] (mM)

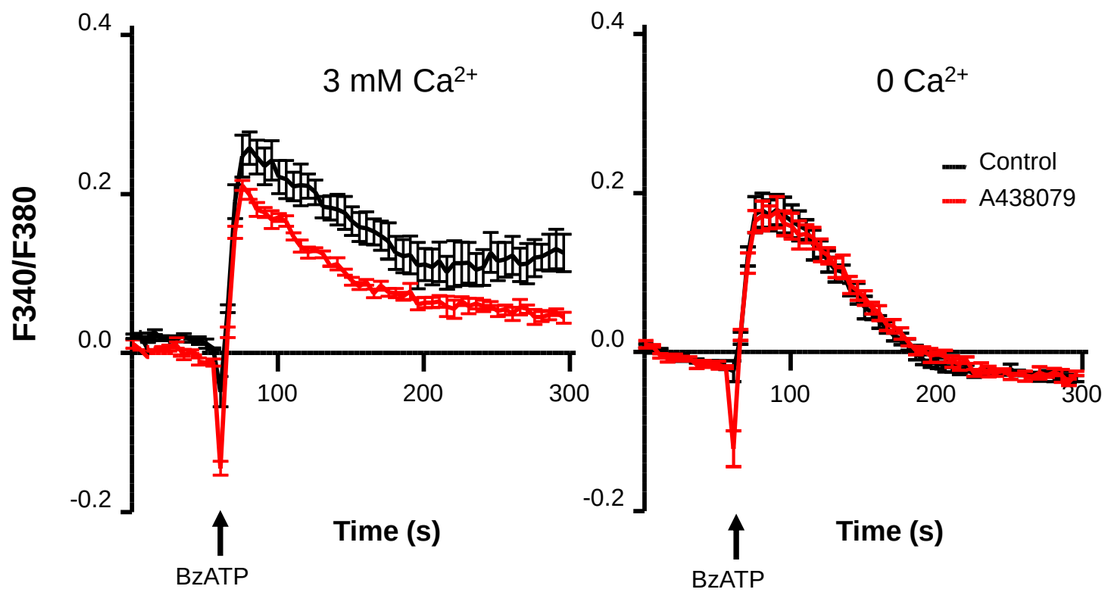
d
3 mM Ca2+
0 Ca2+
F340/F380
Control
A438079
Time (s)
BzATP

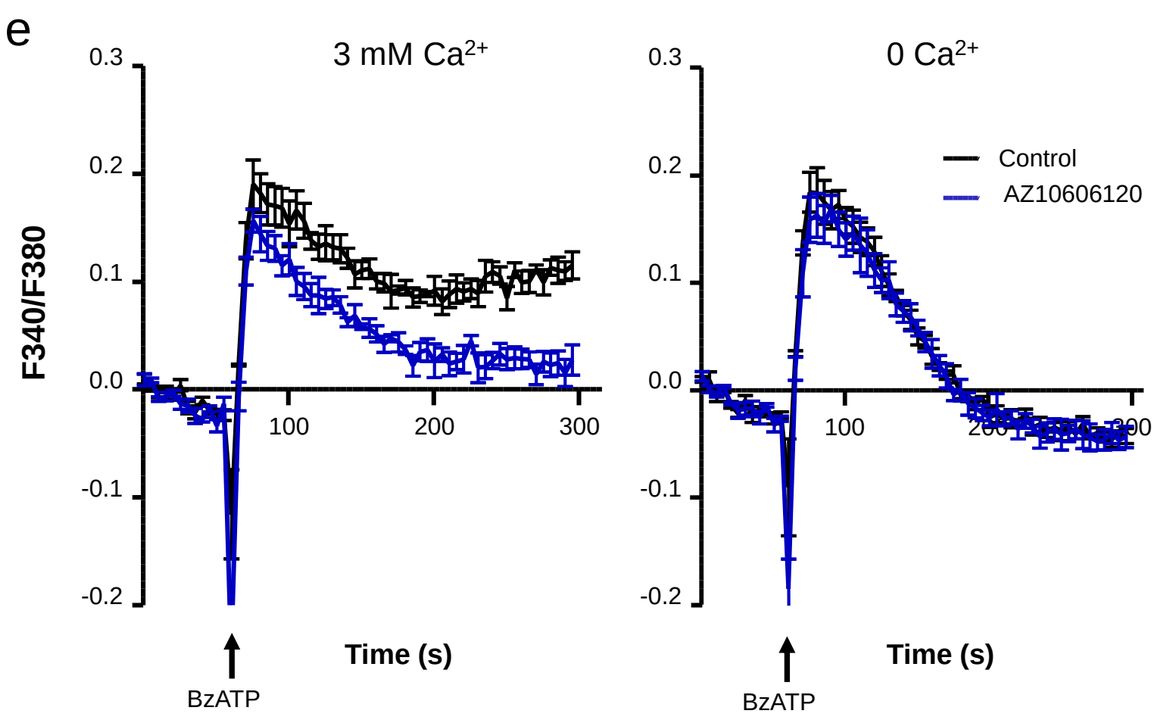
e
3 mM Ca2+
0 Ca2+
F340/F380
Control
AZ10606120
Time (s)
BzATP

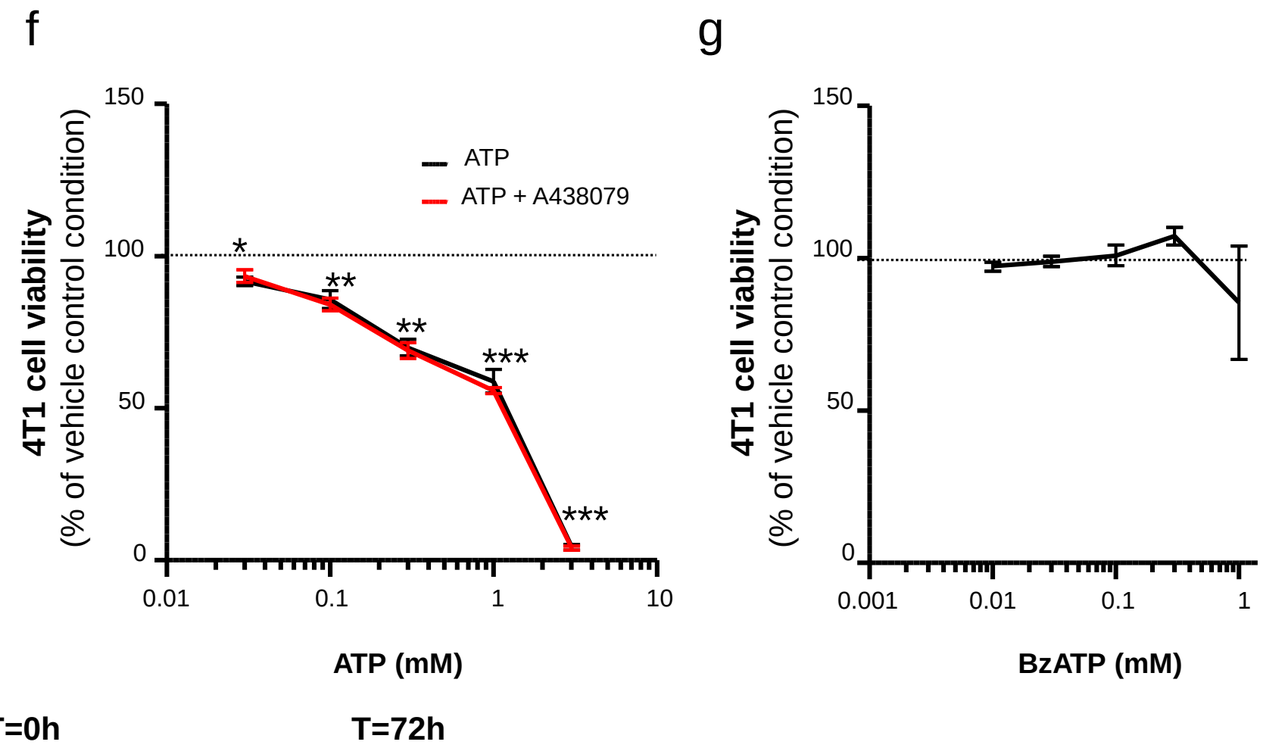
f
g
4T1 cell viability
(% of vehicle control condition)
ATP
ATP + A438079
ATP (mM)
BzATP (mM)

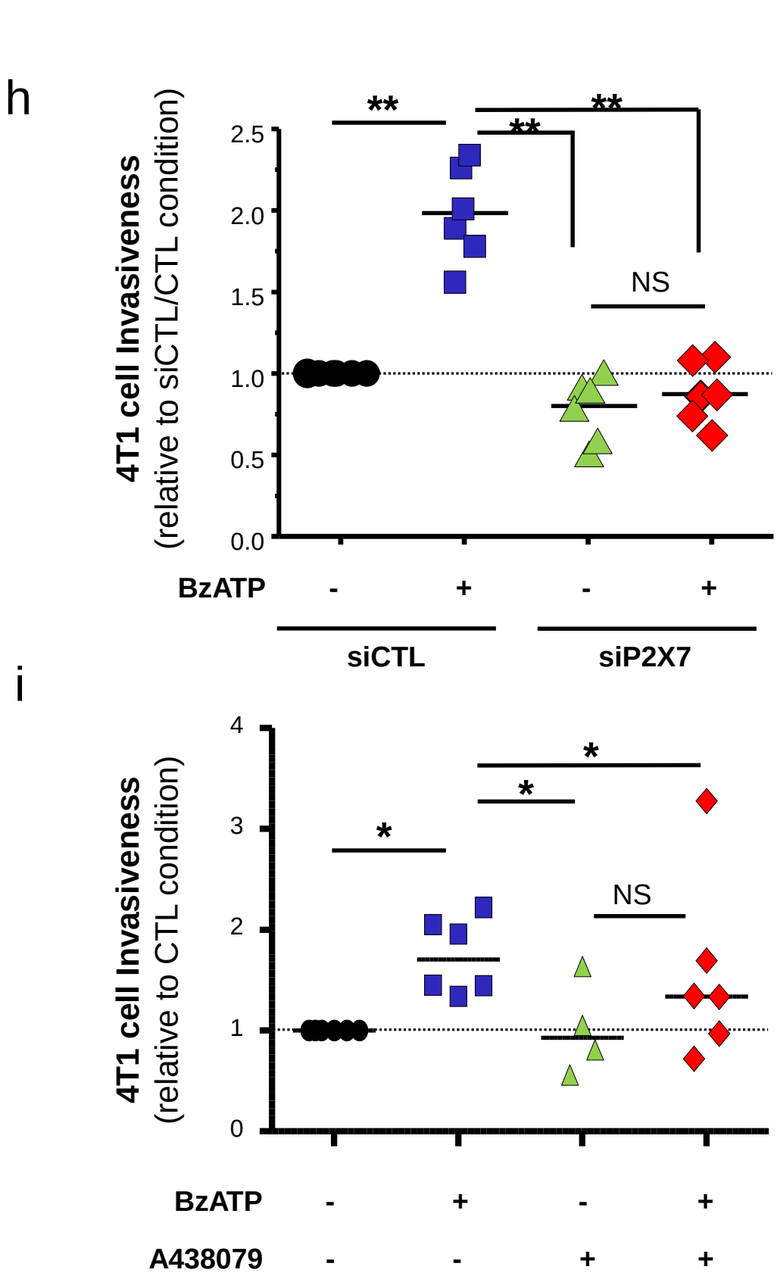
h
i
4T1 cell Invasiveness
(relative to siCTL/CTL condition)
(relative to CTL condition)
BzATP
siCTL
siP2X7
A438079
NS

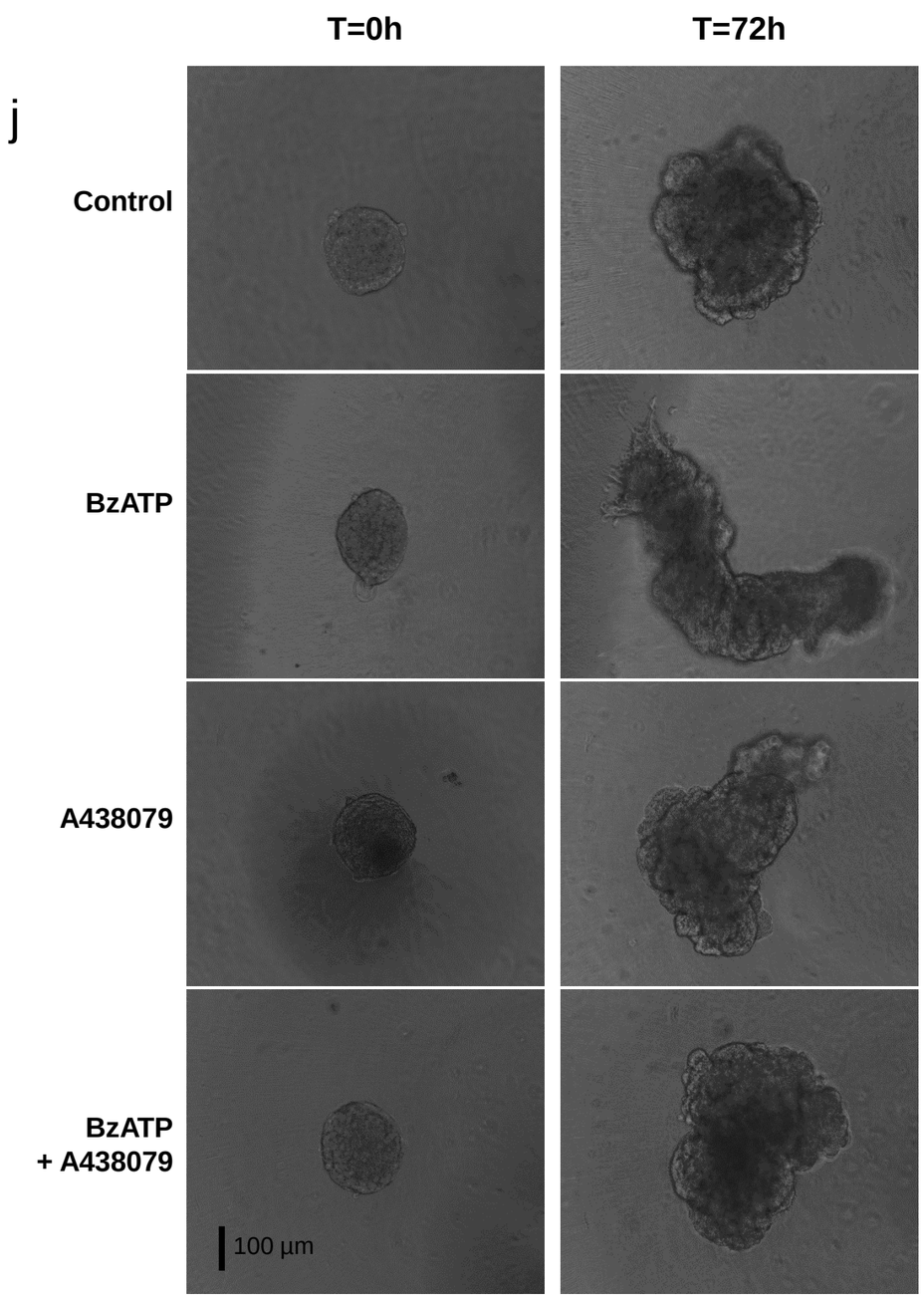
j
T=0h
T=72h
Control
BzATP
A438079
BzATP
+ A438079
100 µm

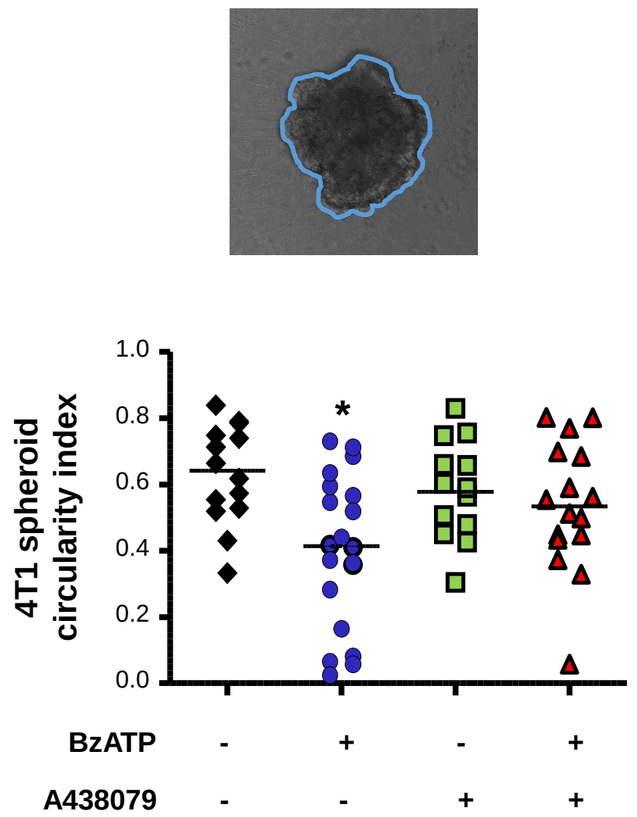
Spheroid Circularity
4T1 spheroid
circularity index
BzATP
A438079

Figure 2

a

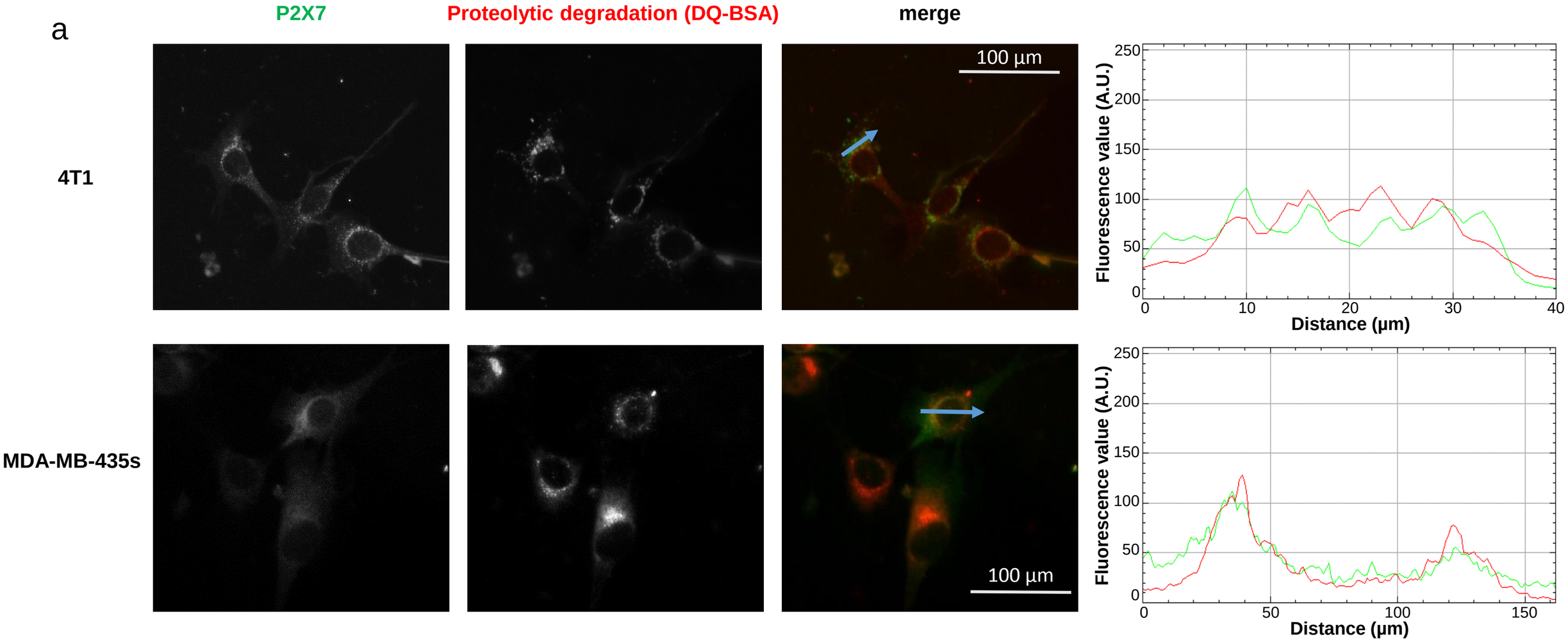

b

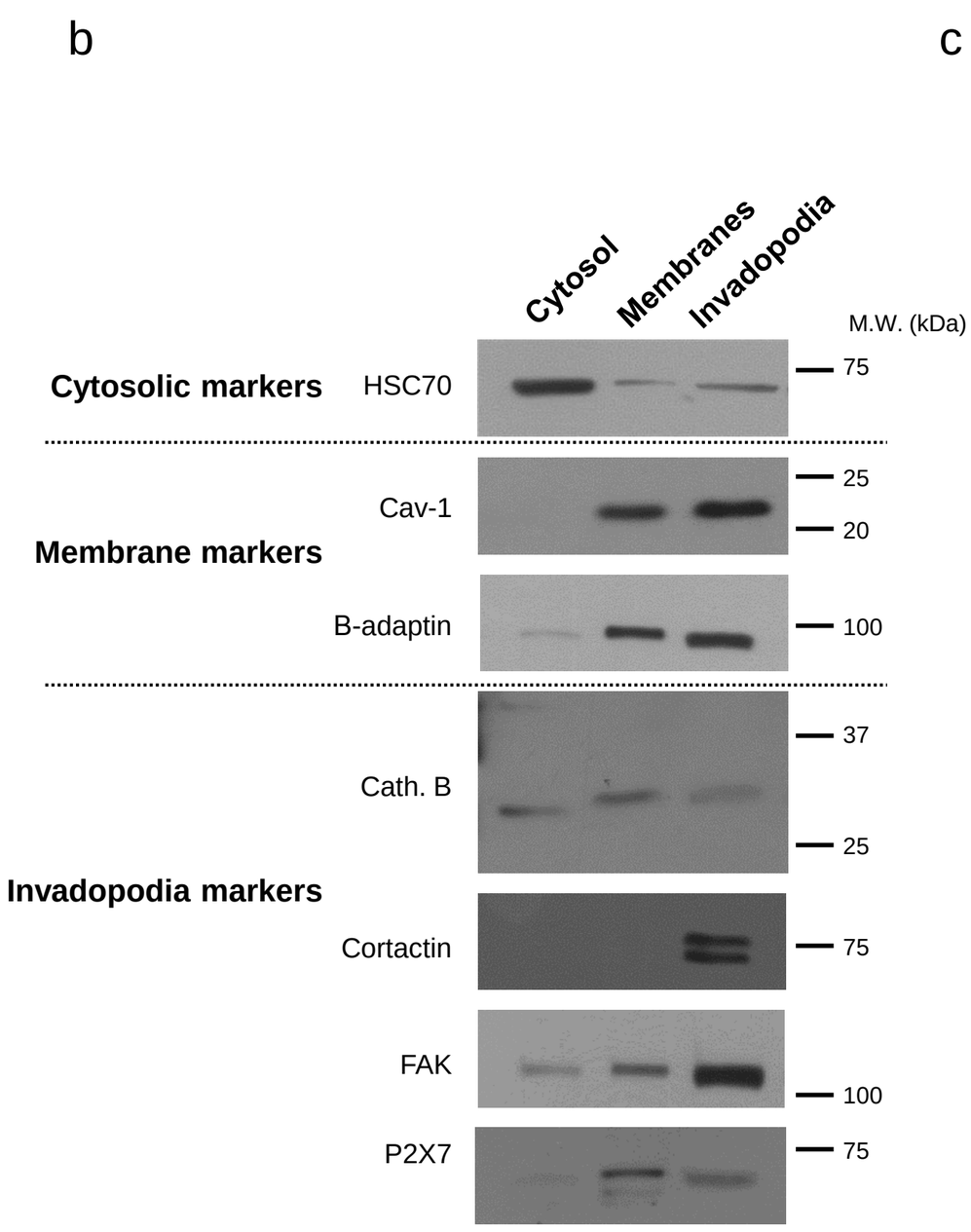

c

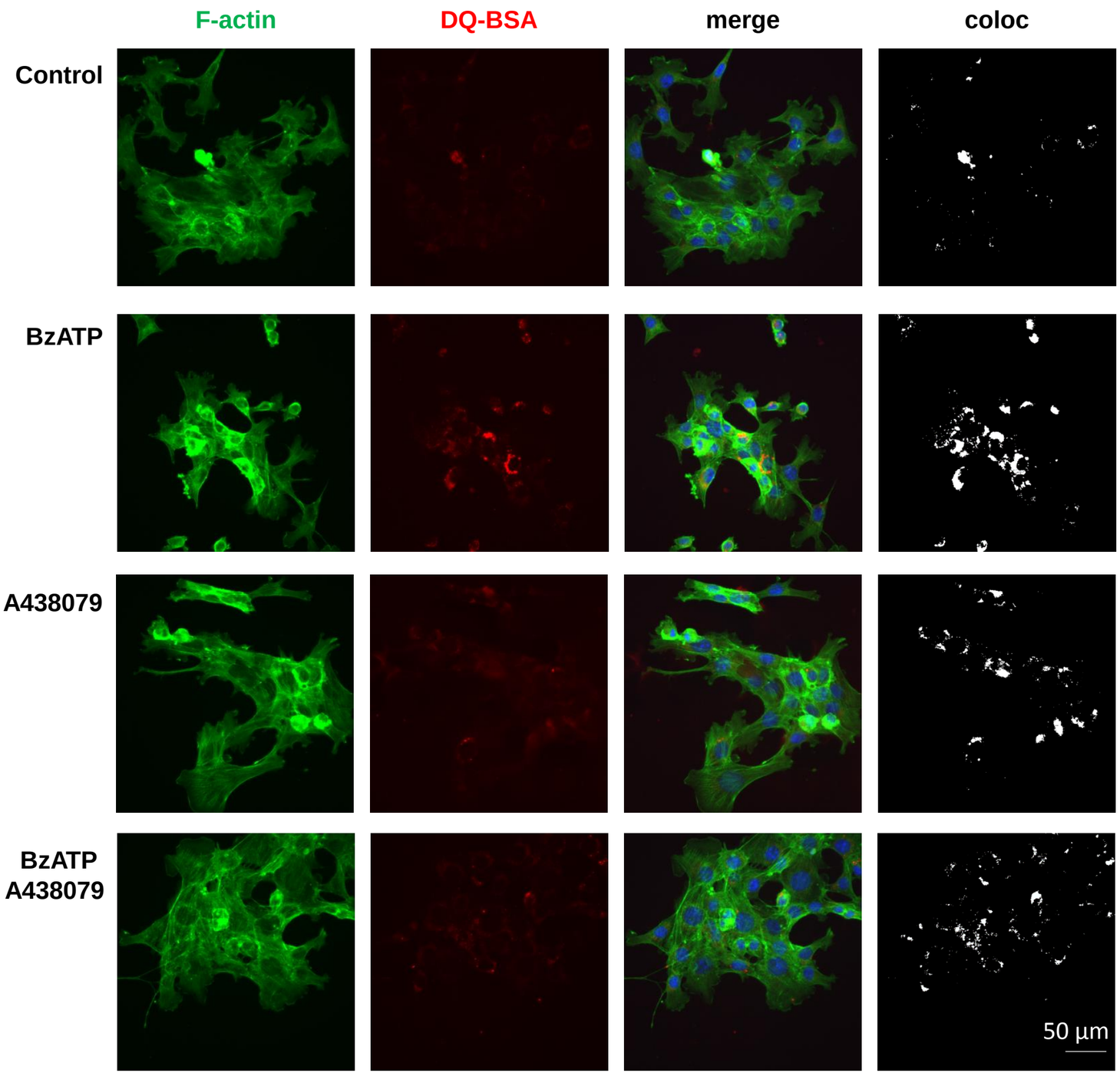

d

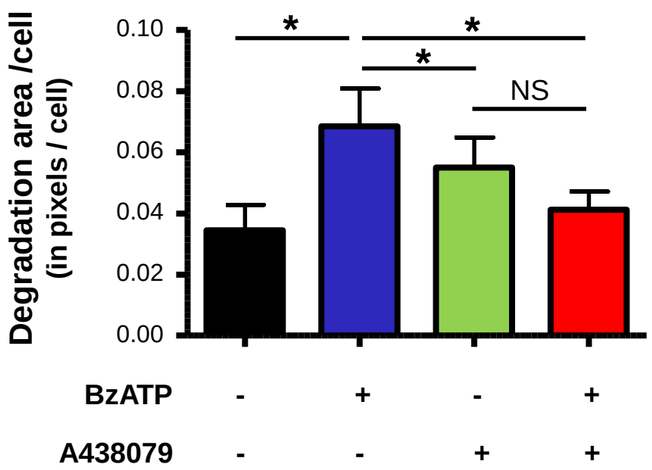

e

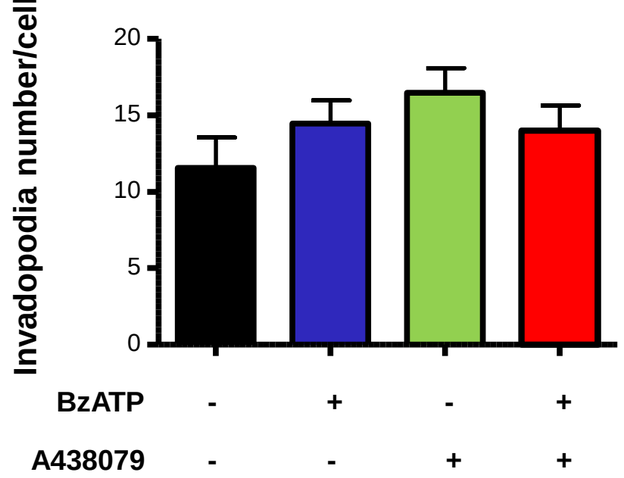

Figure 3

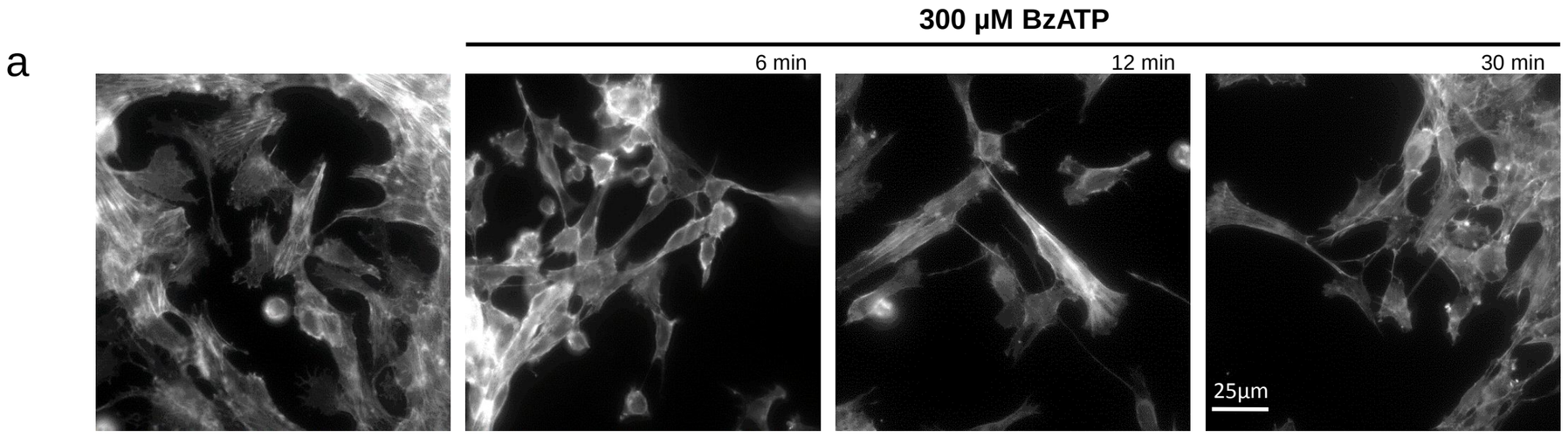
a
300 µM BzATP
6 min
12 min
30 min
25µm
b
Filopodia number / hr
150
100
50
0
*
*
*
NS
BzATP - + - +
A438079 - - + +
c
Filopodia velocity
0.5
0.4
0.3
0.2
0.1
0.0
BzATP - + - +
A438079 - - + +
d
His-CDC42
Total Cdc42
CDC42-GTP
25kDa
25kDa
His-RhoA
Total RhoA
RhoA-GTP
25kDa
25kDa
His-Rac1
Total Rac1
Rac1-GTP
25kDa
25kDa
BzATP - + - +
A438079 - - + +
GTP-bound / total cdc42
8
6
4
2
0
*
*
*
NS
GTP-bound / total RhoA
15
10
5
0
GTP-bound / total Rac1
10
8
6
4
2
0
BzATP - + - +
A438079 - - + +
e
mRNA expression level
Relative to CTL condition w/o BzATP
2.5
2.0
1.5
1.0
0.5
0.0
*
P2rx7
SNAI1
ZEB1
TWIST
ZO1
CDH1

Figure 4

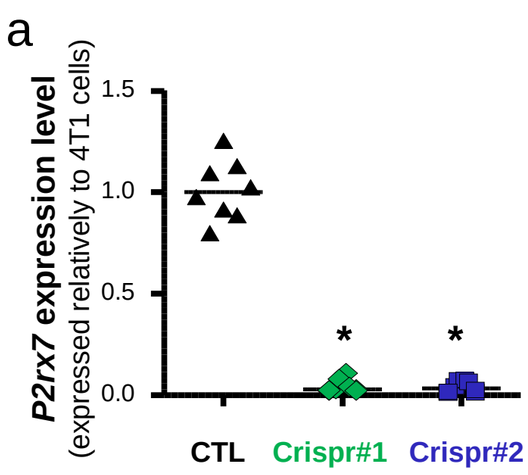
a
P2rx7 expression level
(expressed relatively to 4T1 cells)
1.5
1.0
0.5
0.0
*
*
CTL
Crispr#1
Crispr#2

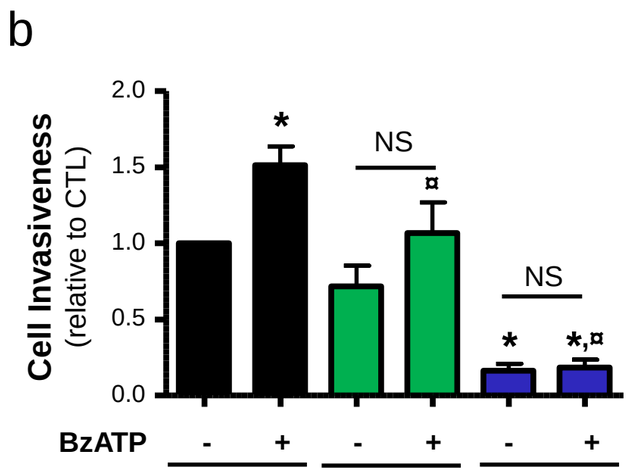
b
Cell Invasiveness
(relative to CTL)
2.0
1.5
1.0
0.5
0.0
*
NS
¤
NS
*
*,¤
BzATP
-
+
-
+
-
+
CTL
Crispr#1
Crispr#2

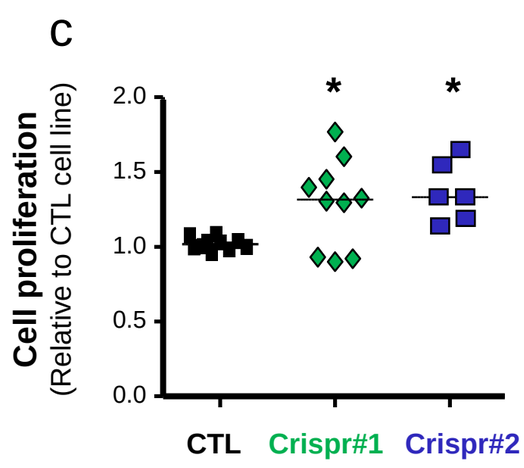
c
Cell proliferation
(Relative to CTL cell line)
2.0
1.5
1.0
0.5
0.0
*
*
CTL
Crispr#1
Crispr#2

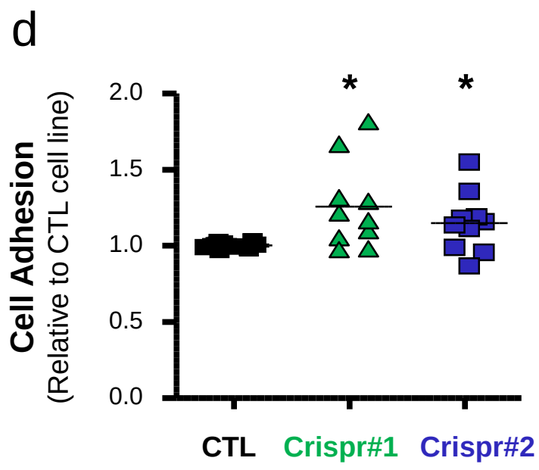
d
Cell Adhesion
(Relative to CTL cell line)
2.0
1.5
1.0
0.5
0.0
*
*
CTL
Crispr#1
Crispr#2

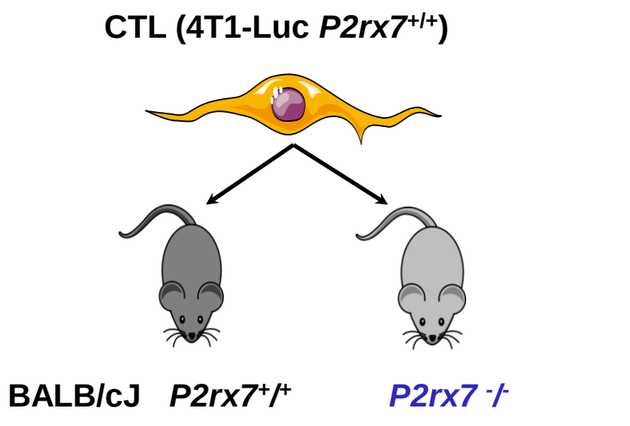
e
CTL (4T1-Luc P2rx7+/+)
BALB/cJ
P2rx7+/+
P2rx7 -/-

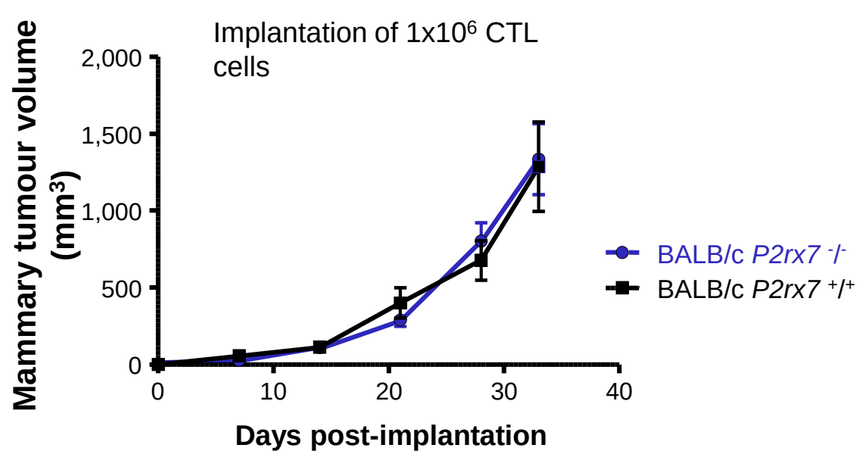
f
Implantation of 1x10⁶ CTL cells
Mammary tumour volume (mm³)
2,000
1,500
1,000
500
0
0
10
20
30
40
Days post-implantation
BALB/c P2rx7 -/-
BALB/c P2rx7 +/+

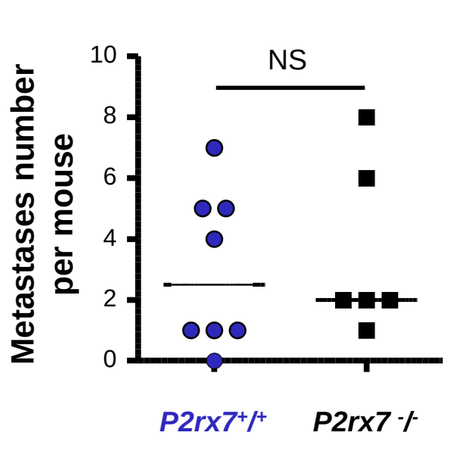
g
Metastases number per mouse
NS
10
8
6
4
2
0
P2rx7+/+
P2rx7 -/-

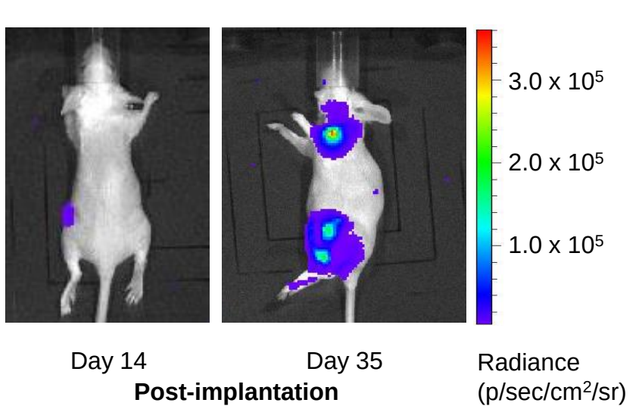
3.0 x 10⁵
2.0 x 10⁵
1.0 x 10⁵
Day 14
Day 35
Post-implantation
Radiance
(p/sec/cm²/sr)

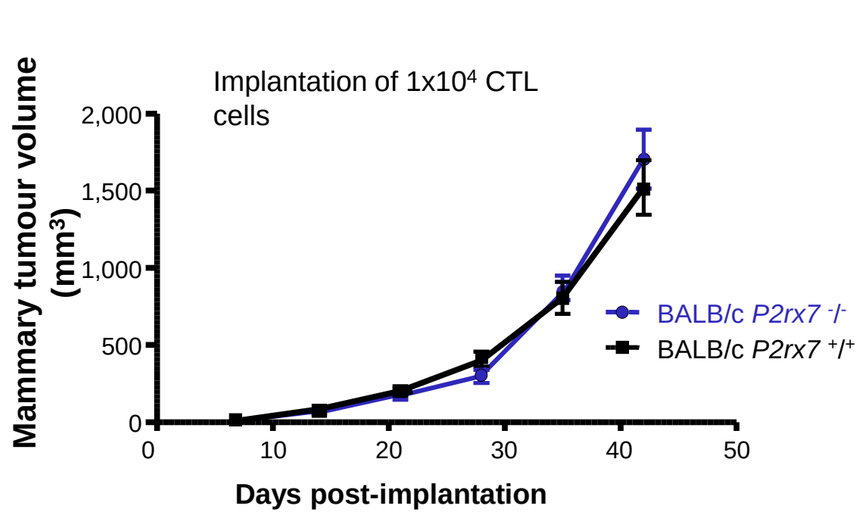
h
Implantation of 1x10⁴ CTL cells
Mammary tumour volume (mm³)
2,000
1,500
1,000
500
0
0
10
20
30
40
50
Days post-implantation
BALB/c P2rx7 -/-
BALB/c P2rx7 +/+

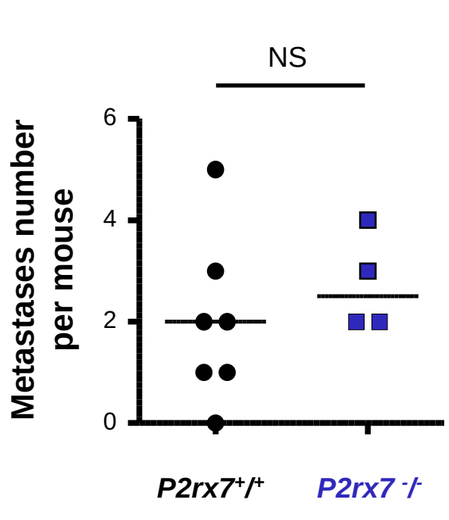
i
NS
Metastases number per mouse
6
4
2
0
P2rx7+/+
P2rx7 -/-

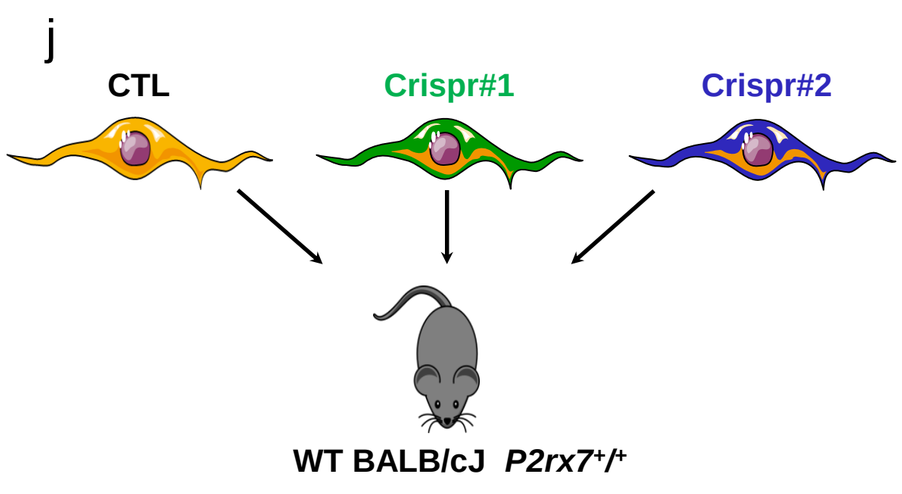
j
CTL
Crispr#1
Crispr#2
WT BALB/cJ P2rx7+/+

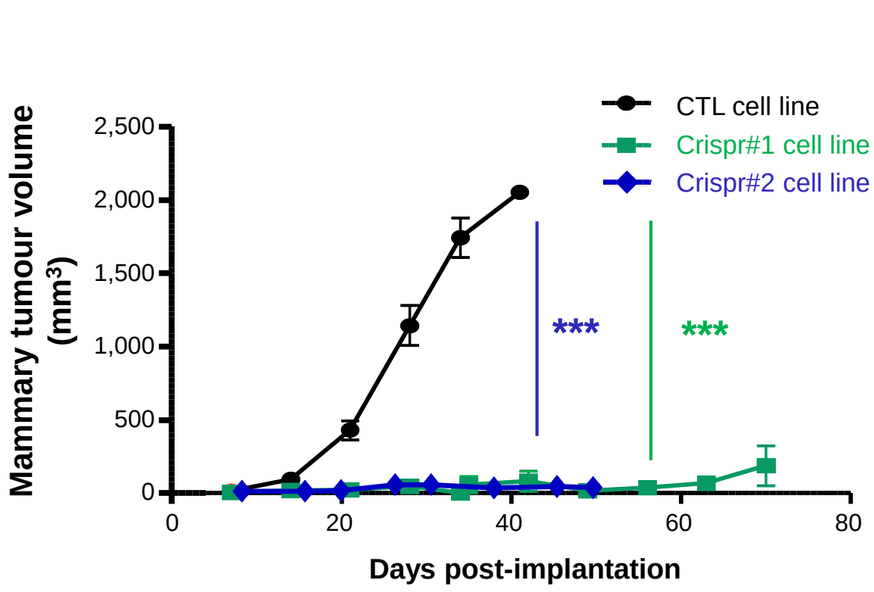
k
Mammary tumour volume (mm³)
2,500
2,000
1,500
1,000
500
0
0
20
40
60
80
Days post-implantation
CTL cell line
Crispr#1 cell line
Crispr#2 cell line
***
***

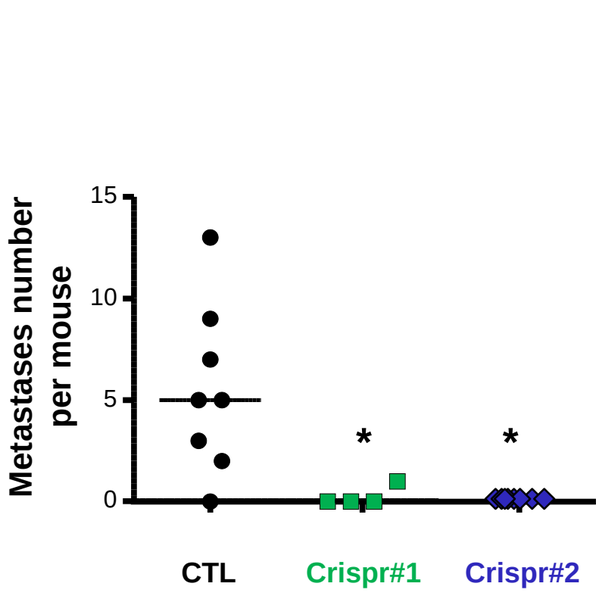
l
Metastases number per mouse
15
10
5
0
*
*
CTL
Crispr#1
Crispr#2

Figure 5

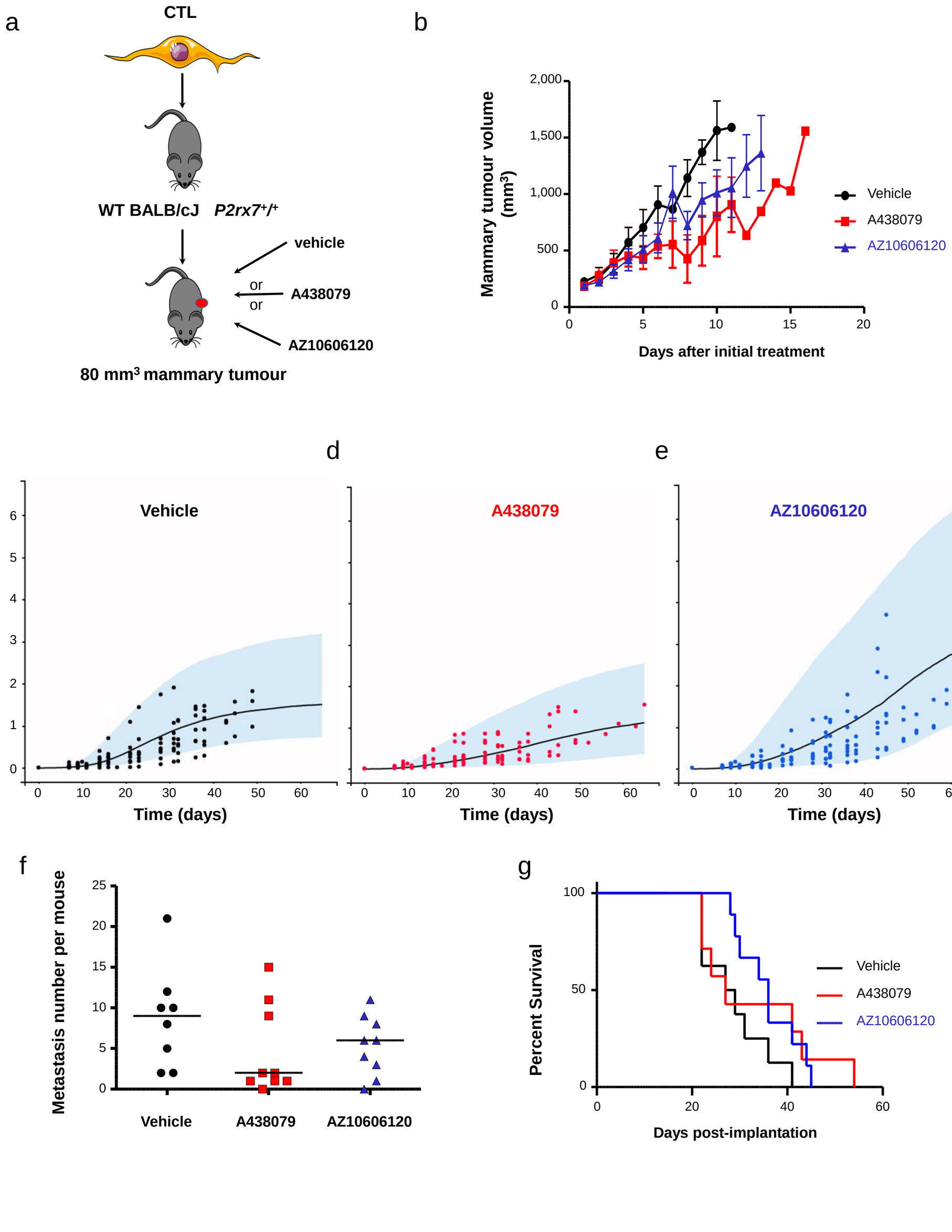
a
CTL
WT BALB/cJ P2rx7+/+
vehicle
or
A438079
or
AZ10606120
80 mm3 mammary tumour
b
Mammary tumour volume (mm3)
2,000
1,500
1,000
500
0
0
5
10
15
20
Days after initial treatment
Vehicle
A438079
AZ10606120
c
d
e
Vehicle
A438079
AZ10606120
Mammary tumour volume (x10³ mm³)
Time (days)
Time (days)
Time (days)
f
Metastasis number per mouse
Vehicle
A438079
AZ10606120
g
Percent Survival
Days post-implantation
Vehicle
A438079
AZ10606120

Table I: PCR primers sequences and expected amplicon size

Mouse genes		Corresponding proteins	Forward primers (5' → 3')	Reverse primers (5' → 3')	Amplicon - Expected size (bp)
Primers for conventional PCR					
mP2rx1	PCR	P2X1	CCTCAAGTGGCCTTATCAGC	GGTACCATTCACCTCCTCCA	467
mP2rx2	PCR	P2X2	ACGTTCATGAACAAAAACAAG	TCAAAGTTGGGCCAAACCTTTGG	360
mP2rx3	PCR	P2X3	GGACGCTATGCCAACAGAGT	ACGTCCCCTACCCTCAAGAT	461
mP2rx4	PCR	P2X4	GCGTCTGTGAAGACCTGTGA	GCCTTTCCAAACACGATGAT	521
mP2rx5	PCR	P2X5	TCCCGGATGGCGAGTGTTCAG	GATGGGGCAGTAGAGATTGGTGGAG	323
mP2rx6	PCR	P2X6	AACTGGGAACATGGCTTCTG	CACCAGCTCCAGATCTCACA	516
mP2rx7	PCR	P2X7	TGCACATGATCGTCTTTTCC	GGCAAGATGTTTCTCGTGGT	532
Primers for real-time qPCR					
mP2rx7	qPCR	P2X7	AGCACGAATTATGGCACCGT	CCCCACCCTCTGTGACATTCT	172
mCDH1	qPCR	E-Cadherin	CAGTTCCGAGGTCTACACCTT	TGAATCGGGAGTCTTCCGAAAA	131
mGusb	qPCR	β-Glucuronidase	TATGGAGCAGACGCAATCCC	TTCGTCATGAAGTCGGCGAA	164
mSnai1	qPCR	Snail1	CACACGCTGCCTTGTGTCT	GGTCAGCAAAAGCACGGTT	133
mTwist	qPCR	Twist	TTCTCGGTCTGGAGGATGGA	TCTCTGGAAACAATGACATCTAGG	110
mZeb1	qPCR	Zeb1	ACCGCCGTCATTTATCCTGAG	CATCTGGTGTTCCGTTTTCATCA	91
mZO1	qPCR	ZO1	GCCTCAGAAATCCAGCTTCTCGAA	GCAGCTAGCCAGTGTACAGTATAC	194